Inorg. Chem. **2006**, *45*, 6246–6262

The Very Covalent Diammino(*o*-benzoquinonediimine) Dichlororuthenium(II). An Example of Very Strong π-Back-Donation

Julia Rusanova,[†] Eduard Rusanov,[†] S. I. Gorelsky,*[,‡] Dharamdat Christendat,[†] Raluca Popescu,[†] Abdiaziz A. Farah,[†] Rémi Beaulac,[§] Christian Reber,[§] and A. B. P. Lever*[,†]

Department of Chemistry, York University, CB124, 4700 Keele Street, Toronto, Ontario M3J 1P3, Canada, Department of Chemistry, Stanford University, 333 Campus Drive, Stanford, California 94305, and Département de Chimie, Université de Montréal, C.P. 6128, Succ. Centre-ville, Montréal, QC H3C 3J7, Canada

Received February 8, 2006

The syntheses and X-ray structures of the complexes $Ru(S\text{-}dmso)Cl_2(opda)$ (**1**) and $Ru(NH_3)_2Cl_2(bqdi)$ (**2**) are described (opda= *o*-phenylenediamine, bqdi= *o*-benzoquinonediimine). Optical absorption and emission, vibrational (resonance Raman), and electrochemical data are discussed. We explore the nature of the ruthenium benzoquinone electronic interaction in species **2** primarily within the framework of density functional theory (DFT) but also using INDO/S to extract Coulombic and exchange integrals. The resonance Raman and emission data were understood in terms of a common set of coupled vibrations localized primarily within the ruthenium metallacycle ring. Experimental and computational data were also compared among a select group of ruthenium bqdi species with other spectator ligands, specifically ammonia, 2,2′-bipyridine, and 2,4-pentanedione. The changes in the electrochemistry, optical spectroscopy, and vibrational spectra with changing spectator ligand donicity were explained within a common theoretical (DFT) model which further provided a detailed analysis of the variation in the molecular orbital descriptions. With the application of an extended charge decomposition analysis (ECDA), a detailed picture emerged of the bonding between the bqdi ligand and the metal atom, illustrating the coupling between the orbitals of each fragment as a function of orbital symmetry and charge transfer between the fragments of the complex. Metal-to-bqdi π-back-donation is seen to be very important.

Introduction

The ligand *o*-benzoquinonediimine (bqdi) and its derivatives are of considerable interest because of the extensive delocalization of Ru 4d electron density over the bqdi ligand.[1−9] This delocalization may be discussed in terms of metal and ligand orbital mixing or donor−acceptor electronic coupling. The covalent interactions between the metal and the ligand can be separated into ligand-to-metal donation (σ and π) and metal-to-ligand π-back-donation.[10,11] The latter can be estimated in terms of the Ru 4dπ contribution to the bqdi π* LUMO. Alternatively, one may consider the π* unoccupied orbital contributions in the occupied Ru 4dπ orbitals. Density functional theory at the B3LYP/LanL2DZ level shows that there is 21% Ru character in LUMO+1,2 of the $[Ru(bqdi)_3]^{2+}$ cation[12] (the π* LUMO does not mix with Ru 4dπ orbitals for symmetry reasons). Considering that the Ru contribution is distributed over three bqdi ligands, we arrive at ca. $21 \times 2/3 = 14\%$ Ru contribution per bqdi

* To whom correspondence should be addressed. E-mail: blever@yorku.ca (A.B.P.L.); sg@sg-chem.net (S.I.G.).
[†] York University.
[‡] Stanford University.
[§] Université de Montréal.

(1) Masui, H.; Lever, A. B. P.; Dodsworth, E. S. *Inorg. Chem.* **1993**, *32*, 258.
(2) Da Cunha, C. J.; Fielder, S. S.; Stynes, D. V.; Masui, H.; Auburn, P. R.; Lever, A. B. P. *Inorg. Chim. Acta* **1996**, *242*, 293.
(3) Metcalfe, R. A.; Dodsworth, E. S.; Fielder, S. S.; Stufkens, D. J.; Lever, A. B. P.; Pietro, W. J. *Inorg. Chem.* **1996**, *35*, 7741.
(4) Metcalfe, R. A.; Lever, A. B. P. *Inorg. Chem.* **1997**, *36*, 4762.
(5) Gorelsky, S. I.; Dodsworth, E. S.; Lever, A. B. P.; Vlcek, A. A. *Coord. Chem. Rev.* **1998**, *174*, 469.
(6) Lever, A. B. P.; Gorelsky, S. I. *Coord. Chem. Rev.* **2000**, *208*, 153.
(7) Gorelsky, S. I.; Lever, A. B. P. *Can. J. Anal. Sci. Spectrosc.* **2003**, *48*, 93.
(8) Venegas-Yazigi, D.; Mirza, H.; Lever, A. B. P.; Lough, A. J.; Costamagna, J.; LaTorre, R. *Acta Crystallogr.* **2000**, *C56*, e281.
(9) Sizova, O. V.; Ivanova, N. V.; Ershov, A. Y. *Russ. J. Gen. Chem.* **2001**, *71*, 1501.
(10) Chatt, J.; Duncanson, L. *J. Chem. Soc.* **1953**, 2939.
(11) Dewar, M. J. S. *Bull. Chim. Soc. Fr.* **1951**, C73.
(12) Gorelsky, S. I.; Lever, A. B. P. *J. Organomet. Chem.* **2001**, *635*, 187.

10.1021/ic060220z CCC: $33.50
Published on Web 07/06/2006

ligand. The Ru character in LUMO+1,2 of $[Ru(bpy)_3]^{2+}$ (bpy = 2,2′-bipyridine) is 6%, leading to ca. 4% Ru contribution per ligand.[12] 2,2′-Bipyridine is often regarded as a good π-accepting ligand but one may see from these data that bqdi is much better. More illustrative is a comparison of $[Ru(NH_3)_4(bqdi)]^{2+}$ with $[Ru(NH_3)_4(bpy)]^{2+}$ where a common $[Ru(NH_3)_4]^{2+}$ fragment donates to a single bqdi or bpy ligand. The Ru contributions to the LUMO here are 21 and 5%, respectively.[13,14] Thus, bqdi takes advantage of the extra electron "richness" when more strongly donating spectator ligands replace weakly donating ones. On the basis of ligand electrochemical parameters,[15,16] the Ru^{II} ion in the tetraammine species is ca. 0.75 V easier to oxidize than in the bis(bipyridine) species. The behavior of bqdi can be associated with the redox activity of these ligands. While both bpy and bqdi can form monoanions, the benzosemiquinonediimine is much more accessible (stable) (when bound to a metal ion) than the bipyridine monoanion.

This raises several questions: (i) if the Ru^{II} center is made more electron rich, can Ru-to-L π-back-donation and, as a consequence, the Ru 4dπ contribution to the LUMO be dramatically increased, possibly to a maximum covalent contribution (i.e., 50%), (ii) can a more detailed description of the electronic structure and orbital interactions be derived for these Ru^{II} complexes to gain greater insight into their molecular structures, and (iii) what new spectroscopic and electrochemical properties might a system with greatly enhanced Ru-to-L π-back-donation exhibit.

To explore these questions, we report the synthesis and properties of the $[Ru^{II}(NH_3)_2Cl_2(bqdi)]$ species which, on the basis of its ligand electrochemical parameters,[15] is ca. 0.34 V easier to oxidize than $[Ru^{II}(NH_3)_4(bqdi)]^{2+}$. In this new species, Ru-to-bqdi π-back-donation increased to 32% Ru 4dπ contribution to the LUMO, indicating a transfer of ~0.7 electrons to the bqdi ligand in the electronic ground state. The characterization of this species including optical (absorption and emission), vibrational (resonance Raman), and mass spectra, electrochemical and spectroelectrochemical behavior, crystal structure determination and electronic structure analysis using density functional theory (DFT), and time-dependent DFT (TD-DFT) is reported here. The combination of computational methods and resonance Raman spectroscopy is a particularly powerful means of elucidating the detailed structures of metal complexes (e.g., refs 17−24). The compound has been briefly described.[25,26]

Recently developed extended charge decomposition analysis (ECDA)[27] and Mayer bond orders[28,29] are used to analyze orbital interactions. These methods allow a detailed understanding of the chemical bonding in terms of symmetry (σ, π, and δ interactions) and the nature of the electronic interactions (electron donation and π-back-donation between the fragments and electronic polarization of the fragments) being enhanced by spectator ligand donation to the metal to be extracted.

Experimental Section

Methods and Materials. All reagents were obtained from Aldrich Chemicals Canada, Fluka Inc., Alfa Aesar, and Johnson Matthey Company. Reagent grade and HPLC grade solvents were obtained from Caledon and BDH Inc. All chemicals and solvents were purified when necessary according to standard laboratory techniques.

Equipment. ^1H and ^{13}C NMR spectra were obtained on a Bruker ARX 300 nuclear magnetic resonance spectrometer in DMSO-d_6 using tetramethylsilane as an internal standard. Signals are described as singlets (s), doublets (d), doublets of doublets (dd), triplets (t), quartets (q), pentets (p), sextets (s), broad (br), or multiplets (m). Infrared (IR) spectra were recorded as KBr pellets with a Mattson 3000 FTIR Spectrophotometer.

Raman spectra were measured using a Renishaw 3000 Raman imaging microscope and the 488 nm excitation line of an Ar^+ ion laser (see Table S1). The microscope was used to focus the light onto a spot of approximately 1 μm in diameter and to collect the scattered light. The backscattered Raman light was detected with a Peltier cooled CCD detector. This instrument was also used to collect luminescence from the sample. Lifetime data were taken using a pulsed Nd:YAG laser (Continuum Minilite II). The frequency of the fundamental line was doubled to excite the sample with a 532 nm pulse. Emitted light was then dispersed using a 0.5 m Spex500 monochromator equipped with a 600 grooves mm^{-1} grating and detected with a Hamamatsu R928 opaque photocathode tube cooled to −40 °C (Products for Research thermoelectric refrigerated chamber TF177RF) to reduce the dark noise level. Lifetime data were monitored on a digital oscilloscope (Tektronix TDS380). The temperature of the samples was controlled with an Oxford Instruments CF-1204 He gas-flow cryostat. Low-temperature solid-state resonance Raman spectra were recorded using a Princeton Instruments, liquid nitrogen-cooled back-illuminated CCD camera mounted on a Spex 1877 0.6 m triple spectrometer, equipped with holographic grating blazed at 1200, 1800, or 2400 grooves mm^{-1}. An Ar ion (Sabre-25/7) 501 nm laser line was used for

(13) Lever, A. B. P.; Gorelsky, S. I. *Struct. Bonding* **2004**, *107*, 77.
(14) Gorelsky, S. I.; Lever, A. B. P.; Ebadi, M. *Coord. Chem. Rev.* **2002**, *230*, 97.
(15) Lever, A. B. P. *Inorg. Chem.* **1990**, *29*, 1271.
(16) Lever, A. B. P. In *Comprehensive Coordination Chemistry, II;* McCleverty, J. A., Meyer, T. J., Eds.; Elsevier Pergamon: New York, 2003; Vol. 2, p 251.
(17) Li, W.; Wang, Y. B.; Pavel, I.; Yuan, Q.; Ye, Y.; Fu, E.-Q.; Luo, M.-D.; Hu, J.-M.; Kiefer, W. *J. Phys. Chem. A* **2005**, *109*, 2878.
(18) Záliš, S.; Busby, M.; Kotrba, T.; Matousek, P.; Towrie, M.; Vlček A.,, Jr. *Inorg. Chem.* **2004**, *43*, 1723.
(19) Walsh, P. J.; Gordon, K. C.; Lundin, N. J.; Blackman, A. G. *J. Phys. Chem. A* **2005**, *109*, 5933.
(20) Záliš, S.; Amor, N. B.; Daniel, C. *Inorg. Chem.* **2004**, *43*, 7978.
(21) Howell, S. L.; Matthewson, B. J.; Polson, M. I. J.; Burrell, A. K.; Gordon, K. C. *Inorg. Chem.* **2004**, *43*, 2876.
(22) Waterland, M. R.; Howell, S. L.; Gordon, K. C.; Burrell, A. F. *J. Phys. Chem. A* **2005**, *109*, 8826.
(23) Xie, P.; Chen, Y.-J.; Uddin, Md. J.; Endicott, J. F. *J. Phys. Chem. A* **2005**, *109*, 4671.
(24) Gorelsky, S. I.; Basumallick, L.; Vura-Weis, J.; Sarangi, R.; Hedman, B.; Hodgson, K. O.; Fujisawa, K.; Solomon, E. *Inorg. Chem.* **2005**, *44*, 4947.
(25) Rusanova, J.; Rusanov, E.; Lever, A. B. P. Inorganic Discussion Weekend, IDW McMaster University, Hamilton, Ontario, Canada, 2003.
(26) Lever, A. B. P.; Rusanova, J.; Rusanov E.; Gorelsky, S. I.; Beaulac, R.; Reber, R. C. 16th International Conference on the Photochemistry and Photophysics of Coordination Compounds, ISPPCC, Asilomar, CA, 2005.
(27) Gorelsky, S. I.; Ghosh, S.; Solomon, E. I. *J. Am. Chem. Soc.* **2006**, *128*, 278.
(28) Mayer, I. *Chem. Phys. Lett.* **1983**, *97*, 270.
(29) Gorelsky, S. I. *AOMix-L Program*; York University: Toronto, Canada, 2002; http://www.sg-chem.net/aomix-s/.

excitation. A powder sample was loaded in a 2 mm EPR tube and stored in liquid nitrogen. The spectrum was obtained in a ~135° backscattering geometry with 25 mW incident power.

Absorption spectra were measured with a Varian Cary 5E or 2400 spectrometer or Hewlett-Packard 8452A diode array spectrometer.

Electrospray mass spectral data were acquired using an API 2000 (MDS−SCIEX, Concord, ON, Canada) triple quadrupole ($Q_1q_2Q_3$) mass spectrometer in the positive ion mode, equipped with a "turbo ion spray" ion source. Full details are presented elsewhere.[30] Electrochemical data were collected in dimethylformamide with tetraethylammonium hexafluorophosphate as the supporting electrolyte using a Cypress system version 5.5 computer-controlled electroanalysis system (ESA, Inc., Chelmsford, MA). An AgCl/Ag wire was used as a quasireference electrode, and a Pt wire was used as a counter electrode, employing ferrocene as the internal reference.

All crystallographic measurements were performed at 150 K on a Nonius Kappa CCD diffractometer. Intensity data were collected using Mo Kα radiation ($\lambda = 0.71073$ Å). Data were corrected for Lorenz and polarization effects. The structures were solved by direct methods and refined with the full-matrix least-squares technique in the anisotropic approximation for non-hydrogen atoms using the SHELXS97 and SHELXL97 programs.[31] All hydrogen atoms in **1** and NH hydrogen atoms in **2** were located in the difference Fourier maps and refined isotropically, whereas the CH hydrogen atoms in **2** were placed in ideal positions (Table 1).

Full crystallographic parameters have been deposited at Cambridge Crystallographic Data Centre (CCDC). Any request to the CCDC for these materials should quote the full literature citation and reference number CCDC.

Syntheses. $[Ru(S\text{-}DMSO)_4Cl_2]$ was prepared according to a literature procedure.[32]

$[Ru(S\text{-}DMSO)_2Cl_2(opda)]$ (1). $[Ru(DMSO)_4Cl_2]$ (0.50 g, 1.03 mmol) was refluxed in anhydrous ethanol (24 mL) under argon for 20 min. It was then added to an equimolar amount of freshly sublimed *o*-phenylenediamine in 5 mL of the same solvent and further refluxed for 4 h. During the course of reaction, the initial yellow-orange solution gradually turned orange-red. After the reaction mixture was cooled to room temperature, it was filtered, washed copiously with acetone, and vacuum-dried. Yield: 0.42 g (88%) of a light-yellow analytically pure powder. ^{1}H NMR (DMSO-d_6): δ 7.42 (t, 2H, benzene ring, $J = 2.4$ Hz), 7.22 (dd, 2H, benzene ring, $J = 9.0$ Hz and $J = 2.4$ Hz), 6.05 (s, 4H, NH_2), 3.23 (s, 6H, CH_3). IR (KBr pellets, cm^{-1}): ν 3419 (s, broad, OH str), 3273−3083 (m, sharp, N−H str), 2916 (m, sharp, aliph C−H str), 2844 (m, sharp, arom C−H str), 1550 (s, sharp, N−H str), 1480 (m, sharp,C−N str), 1070−1015 (m, broad, S═O str), 970−680 (m, sharp, N−H out-of-plane bend). Anal. Calcd for $C_{10}H_{20}Cl_2N_2O_2RuS_2$: C, 27.5; H, 4.62; N, 6.42. Found: C, 27.3; H, 4.5; N, 6.4.

$[Ru(NH_3)_2Cl_2(bqdi)]$ (2). $[Ru(DMSO)_2Cl_2(opda)]$ (0.35 g) was dissolved in dry CH_2Cl_2 (15 mL), and the mixture was stirred for 20 min at 298 K and then filtered. A saturated anhydrous ammonia/methanol solution (15 mL) was added, and the initial yellow solution immediately turned dark-red. The reaction mixture was stirred for another half hour and later kept in the fridge for 7 days. The resulting analytically pure reaction product was filtered and vacuum-dried. Yield: 0.25 g (96%) of dark-reddish powder. Water must be excluded from this preparative route. ^{1}H NMR (DMSO-d_6): δ 12.15 (s, 2H, NH), 7.43 (dd, 2H, benzene ring, $J = 3.3$ Hz), 6.71 (dd, 2H, benzene ring, $J = 3.2$ Hz), 4.26 (s, 6H, NH_3). IR (KBr pellets, cm^{-1}): ν 3480−3224 (m, sharp, N−H str), 2916 (m, sharp, aliph C−H str), 2848 (m, sharp, arom C−H str), 1521 (s, sharp, N−H str), 1480 (m, sharp,C−N str), 1017−811 (m, sharp, N−H out-of-plane bend). ESI-MS: parent ion 312 *m*/*e* (calcd 312). Anal. Calcd for $C_6H_{12}Cl_2N_4Ru\cdot 2CH_3OH$: C, 25.5; H, 5.36; N, 14.9. Found: C, 25.41; H, 4.29; N, 14.82.

Table 1. Summary of Crystal Data and Refinement Results for $[Ru(DMSO)_2Cl_2(opda)]$ (**1**) and $[Ru(NH_3)_2Cl_2(bqdi)]$ (**2**)

	1	**2**
empirical formula	$C_{10}H_{20}Cl_2N_2O_2RuS_2$	$C_6H_{12}Cl_2N_4Ru$
fw	436.37	312.17
temp (K)	150(1)	150(1)
wavelength (Å)	0.71073	0.71073
cryst dimension (mm)	0.10 × 0.80 × 0.06	0.16 × 0.16 × 0.07
cryst syst	monoclinic	orthorhombic
space group	$P2_1/n$	*Pnma*
unit cell dimensions		
a (Å)	12.629(1)	8.080(2)
b (Å)	8.1826(4)	8.794(2)
c (Å)	15.539(1)	15.173(3)
β (deg)	98.459(2)	
vol (Å^3)	1588.3(2)	1078.1(4)
Z	4	4
calcd density (g cm^{-3})	1.825	1.923
abs coeff (mm^{-1})	1.585	1.911
F(000)	880	616
θ range (deg)	2.65−25.06	2.68−27.53
limiting indices	$15 < h < 14$	$-10 < h < 10$
	$-9 < k < 9$	$-10 < k < 11$
	$-18 < l < 18$	$-17 < l < 19$
reflns collected/unique	15 308/2790	7929/1317
completeness to θ (%)	99.5	99.4
max. and min. transmission	0.923 and 0.819	0.893 and 0.719
abs correction	semiempirical from equivalents	
refinement method	full-matrix least squares on F^2	
data/restraints/params	2790/4/192	1317/0/88
GOF on F^2	1.041	1.058
Final R indices	R1 = 0.0413	R1 = 0.0376
[$I > 2\sigma(I)$]	wR2 = 0.0930	wR2 = 0.0823
R indices	R1 = 0.0619	R1 = 0.0578
(all data)	wR2 = 0.1013	wR2 = 0.0900
largest diff. peak and hole (e Å^{-3})	0.835 and −1.031	0.988 and −1.178

Calculations. Density functional theory (DFT) calculations were performed using the *Gaussian 03* program (revision C.01 and C.02).[33] The spin-restricted method was employed to model the closed-shell species and the spin-unrestricted method was employed

(30) Francis, G.; Orlova, G.; Lever, A. B. P.; Bohme, D. K. Unpublished work.
(31) Sheldrick, G. *Program for Structure Refinement*; University of Göttingen: Göttingen, Germany, 1997.
(32) Evans, I. P.; Spencer, A.; Wilkinson, G. *J. Chem. Soc., Dalton Trans.* **1973**, 204.
(33) Frisch, M. J.; Trucks, G. W.; Schlegel, H. B.; Scuseria, G. E.; Robb, M. A.; Cheeseman, J. R.; Montgomery, J. A., Jr.; Vreven, T.; Kudin, K. N.; Burant, J. C.; Millam, J. M.; Iyengar, S. S.; Tomasi, J.; Barone, V.; Mennucci, B.; Cossi, M.; Scalmani, G.; Rega, N.; Petersson, G. A.; Nakatsuji, H.; Hada, M.; Ehara, M.; Toyota, K.; Fukuda, R.; Hasegawa, J.; Ishida, M.; Nakajima, T.; Honda, Y.; Kitao, O.; Nakai, H.; Klene, M.; Li, X.; Knox, J. E.; Hratchian, H. P.; Cross, J. B.; Bakken, V.; Adamo, C.; Jaramillo, J.; Gomperts, R.; Stratmann, R. E.; Yazyev, O.; Austin, A. J.; Cammi, R.; Pomelli, C.; Ochterski, J. W.; Ayala, P. Y.; Morokuma, K.; Voth, G. A.; Salvador, P.; Dannenberg, J. J.; Zakrzewski, V. G.; Dapprich, S.; Daniels, A. D.; Strain, M. C.; Farkas, O.; Malick, D. K.; Rabuck, A. D.; Raghavachari, K.; Foresman, J. B.; Ortiz, J. V.; Cui, Q.; Baboul, A. G.; Clifford, S.; Cioslowski, J.; Stefanov, B. B.; Liu, G.; Liashenko, A.; Piskorz, P.; Komaromi, I.; Martin, R. L.; Fox, D. J.; Keith, T.; Al-Laham, M. A.; Peng, C. Y.; Nanayakkara, A.; Challacombe, M.; Gill, P. M. W.; Johnson, B.; Chen, W.; Wong, M. W.; Gonzalez, C.; Pople, J. A. *Gaussian 03*, revision C.02; Gaussian, Inc.: Wallingford, CT, 2004.

to model the open-shell species. Optimized geometries were calculated using the B3LYP exchange-correlation functional[34,35] with the LanL2DZ basis set[36−39] (see Tables S2 and S3). Additional calculations with the extended basis set (DZVP for Ru[40] and TZVP[41] for other atoms) were performed to verify the results of B3LYP/LanL2DZ calculations and to calculate the inner-sphere reorganization energies of the MLCT excited states. The calculations with the extended basis set were in agreement with the B3LYP/LanL2DZ calculations and did not show deviations of more that 2−3% in orbital compositions between the two sets of calculations. Tight SCF convergence (10^{-8} au) was used for all calculations. In addition, symmetry was retained with a *yz* plane containing the metal and the bqdi ligand. Vibrational frequency calculations were performed to ensure that the stationary points were minima and to calculate the vibrational spectra. Calculated frequencies and Raman intensities were transformed with the *SWizard* program[42] into simulated spectra using Lorentzian functions with half-widths of 15 cm^{-1}. Wave function stability calculations were performed (using the *stable* keyword in *Gaussian 03*) to confirm that the wave function obtained corresponded to the ground state.

Molecular orbital (MO) compositions and the overlap populations were calculated using the *AOMix* program[12,43] and the Mulliken scheme.[44−47] Atomic charges were calculated using the Mulliken and natural population analyses[48] (MPA and NPA, respectively) as implemented in *Gaussian 03*. The analysis of the MO compositions in terms of occupied and unoccupied fragment molecular orbitals (OFOs and UFOs, respectively), construction of orbital interaction diagrams, the charge decomposition analysis (CDA), and the extended charge decomposition analysis (ECDA) were performed using *AOMix-CDA*.[27] To analyze the chemical bonding between molecular fragments, the Mayer bond orders $\mathbf{B}_{AB}$[28] and its components from orbitals of different symmetry were obtained using *AOMix-L*.[24,29]

Time-dependent DFT (TD-DFT)[49−51] was used to calculate the energies and intensities of the 35−50 lowest-energy electronic transitions. These were transformed with the *SWizard* program[43] into simulated spectra as described before,[52] using Gaussian functions with half-widths of 3000 cm^{-1}. Polarizable continuum model (PCM) calculations using the IEF-PCM scheme[53−55] and water as a solvent were employed to evaluate the solvent effects upon the various properties of the species.

Semiempirical INDO/S[56−64] calculations are employed using HyperChem 7.5 (Hypercube Inc., FL). Default atomic parameters were used except for the parameters of Ru[65] and Cl.[12,66] The overlap weighting factors $\sigma-\sigma$ and $\pi-\pi$ were set at 1.267 and 0.585,[63] and the number of singly excited configurations used was 1250 (e.g., the configurational space of the 25 highest-occupied and 25 lowest-unoccupied MOs). Coulomb and exchange integrals were extracted from the configuration interaction matrix using the SIG-JK program.[7,67]

Results

[Ru(S-DMSO)$_2$Cl$_2$(opda)] (1). Structural data. This S-bonded DMSO precursor to the desired bqdi species is obtained from reaction of [Ru(DMSO)$_4$Cl$_2$] with *o*-phenylenediamine (opda). It forms as the *trans*-dichloro-bis-S-DMSO isomer (Figure 1). Crystal packing diagrams are shown in the Supporting Information (Figure S1).

The Ru atom in the complex has a distorted pseudo-octahedrally coordinated $RuN_2Cl_2S_2$ polyhedron (Figure 1, Table 2). The Ru−N_{opda} distances (av 2.138 Å) are significantly longer than those observed for the Ru−N_{bqdi} bonds in complex **2** (vide infra). The Ru−S_{DMSO} distances (av 2.241 Å) are typical for complexes of ruthenium with S-coordinated DMSO in the coordination sphere.[68−70] The Cl atoms are pushed toward the opda side of the complex with a Cl1−Ru−Cl2 bond angle of 170.5(1)°. The endocyclic N1−Ru−N2 bond angle is 81.0(2)° because of the chelate nature of the opda ligand. The two S−Ru−N bond angles are different (N1−Ru−S1 = 88.2(1)°, N2−Ru−S2 = 97.5(1)°) because of the unsymmetrical orientation of DMSO and also probably for steric reasons. The molecules of **1** in the crystal are connected by NH···Cl H-bonds in 1-D zigzag chains directed along the crystallographic *b* axis.

A strong band at 1071 cm^{-1} in its IR spectrum is indicative of M−S(O) bonding.[71] The species is stable in dry air in the

(34) Lee, C.; Yang, W.; Parr, R. G. *Phys. Rev. B* **1988**, *37*, 785.
(35) Becke, A. D. *J. Chem. Phys.* **1993**, *98*, 5648.
(36) Dunning, T. H., Jr.; Hay, P. J. In *Modern Theoretical Chemistry*; H. F. Schaefer, I., Ed.; Plenum: New York, 1976; Vol. 3, p 1.
(37) Hay, P. J.; Wadt, W. R. *J. Chem. Phys.* **1985**, *82*, 270.
(38) Hay, P. J.; Wadt, W. R. *J. Chem. Phys.* **1985**, *82*, 284.
(39) Hay, P. J.; Wadt, W. R. *J. Chem. Phys.* **1985**, *82*, 299.
(40) Godbout, N.; Salahub, D. R.; Andzelm, J.; Wimmer, E. *Can. J. Chem.* **1992**, *70*, 560.
(41) Schafer, A.; Huber, C.; Ahlrichs, R. *J. Chem. Phys.* **1994**, *100*, 5829.
(42) Gorelsky, S. I. *SWizard Program*, revision 4.2; York University: Ontario, Canada, 1998; http://www.sg-chem.net/swizard/.
(43) Gorelsky, S. I. *AOMix: Program for Molecular Orbital Analysis*; York University: Toronto, Canada, 1997; http://www.sg-chem.net/
(44) Mulliken, R. S. *J. Chem. Phys.* **1955**, *23*, 1833
(45) Mulliken, R. S. *J. Chem. Phys.* **1955**, *23*, 1841.
(46) Mulliken, R. S. *J. Chem. Phys.* **1955**, *23*, 2338.
(47) Mulliken, R. S. *J. Chem. Phys.* **1955**, *23*, 2343.
(48) Reed, A. E.; Curtiss, L. A.; Weinhold, F. *Chem. Rev.* **1988**, *88*, 899.
(49) Stratmann, R. E.; Scuseria, G. E.; Frisch, M. J. *J. Chem. Phys.* **1998**, *109*, 8218.
(50) Bauernschmitt, R.; Ahlrichs, R. *Chem. Phys. Lett.* **1996**, *256*, 454.
(51) Casida, M. E.; Jamorski, C.; Casida, K. C.; Salahub, D. R. *J. Chem. Phys.* **1998**, *108*, 4439.
(52) Gorelsky, S. I. In *Comprehensive Coordination Chemistry II;* McCleverty, J. A., Meyer, T. J., Eds.: Elsevier Pergamon: New York, 2003; Vol. 2, Chapter 2.51, p 651.
(53) Cances, M. T.; Mennucci, B.; Tomasi, J. *J. Chem. Phys.* **1997**, *107*, 3032.
(54) Mennucci, B.; Tomasi, J. *J. Chem. Phys.* **1997**, *106*, 5151.
(55) Cossi, M.; Barone, V.; Mennucci, B.; Tomasi, J. *Chem. Phys. Lett.* **1998**, *286*, 253.
(56) Ridley, J.; Zerner, M. C. *Theor. Chim. Acta* **1973**, *32*, 111.
(57) Ridley, J.; Zerner, M. C. *Theor. Chim. Acta* **1976**, *42*, 223.
(58) Zerner, M. C.; Loew, G. H.; Kirchner, R. F.; Mueller-Westerhoff, U. T. *J. Am. Chem. Soc.* **1980**, *102*, 589.
(59) Anderson, W. P.; Edwards, W. D.; Zerner, M. C. *Inorg. Chem.* **1986**, *25*, 2728.
(60) Anderson, W. P.; Cundari, T. R.; Zerner, M. C. *Int. J. Quantum Chem.* **1991**, *1991*, 31.
(61) Zerner, M. C. *Reviews In Computational Chemistry*; VCH Publishers: New York, 1991; Vol. 2, p 313.
(62) Stavrev, K. K.; Zerner, M. C.; Meyer, T. J. *J. Am. Chem. Soc.* **1995**, *117*, 8684.
(63) Zerner, M. C. *Metal−Ligand Interactions*; Russo, N.; Salahub, D. R. E. Eds.; Kluwer Academic Publishers: Norwell, MA, 1996; p 493.
(64) Zerner, M. C. *ZINDO Program*, version 98.1; Quantum Theory Project, University of Florida: Gainesville, FL, 1998.
(65) Kroghjespersen, K.; Westbrook, J. D.; Potenza, J. A.; Schugar, H. J. *J. Am. Chem. Soc.* **1987**, *109*, 7025.
(66) Gorelsky, S. I.; Kotov, V. Y. *Russ. J. Coord. Chem.* **1998**, *24*, 491.
(67) Gorelsky, S. I. *SIG-JK Program*; York University: Ontario, Canada, 1998; http://www.sg-chem.net/sig-jk/.
(68) Calligaris, M. *Coord. Chem. Rev.* **2004**, *248*, 351.
(69) Otero, L.; Noblia, P.; Gambino, D.; Cerecetto, H.; Gonzalez, M.; Ellena, J. A.; Piro, O. E. *Inorg. Chim. Acta* **2003**, *344*, 85.
(70) Ilangovan, G.; Pal, R.; Zweier, J. L.; Kuppusamy, P. *J. Phys. Chem. B* **2002**, *106*, 11929.
(71) Cotton, F. A.; Francis, R.; Horrocks, J. W. D. *J. Phys. Chem.* **1960**, *64*, 1534.

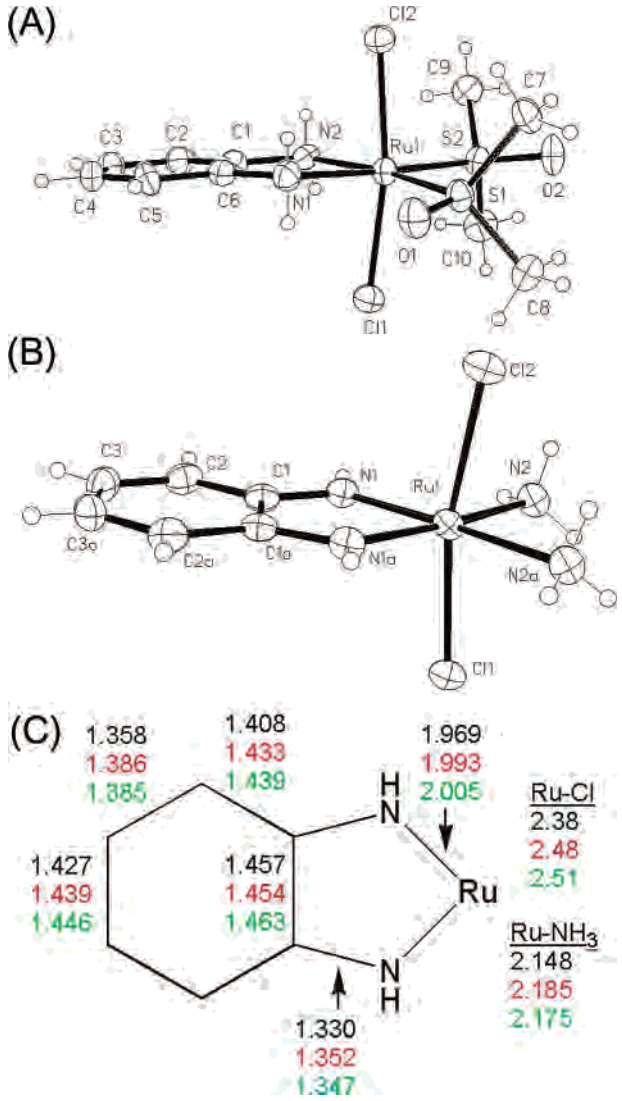

Figure 1. ORTEP diagrams of (A) [Ru(S-DMSO)Cl_2(opda)] (**1**) and (B) [Ru(NH_3)$_2Cl_2$(bqdi)] (**2**) and (C) bond distances (Å) within the bqdi ligand and Ru metallacycle of (**2**): X-ray distances (top), gas-phase DFT-optimized (middle, red) (also see Table S3), and DFT/PCM-optimized (bottom, green).

Table 2. Selected Bond Distances (Å) and Angles (deg) for [Ru(DMSO)$_2Cl_2$(opda)] (**1**)

Ru1−N1	2.128(4)	N1−Ru1−S2	176.9(1)
Ru1−N2	2.148(4)	N2−Ru1−S2	97.5(1)
Ru1−S1	2.233(1)	S1−Ru1−S2	93.45(4)
Ru1−S2	2.250(1)	N1−Ru1−Cl1	87.1(1)
Ru1−Cl1	2.404(1)	N2−Ru1−Cl1	86.2(1)
Ru1−Cl2	2.413(1)	S1−Ru1−Cl1	90.54(4)
S1−O1	1.493(3)	S2−Ru1−Cl1	95.46(4)
S2−Ru1−Cl1	1.494(3)	N1−Ru1−Cl2	85.6(1)
		N2−Ru1−Cl2	86.6(1)
		N1−Ru1−N2	81.0(2)
		N1−Ru1−S1	88.2(1)
		N2−Ru1−S1	168.9(1)
		S1−Ru1−Cl2	95.31(4)
		S2−Ru1−Cl2	91.69(4)
		Cl1−Ru1−Cl2	170.5(1)

solid state but oxidizes in air slowly over a period of hours in neutral solvents. In the presence of O_2 and free base (to deprotonate the opda ligand), it oxidizes rapidly in solution. It is a useful starting point for the synthesis of mono-bqdi ruthenium species.

Optical Spectrum. Complex **1** is a yellow species with

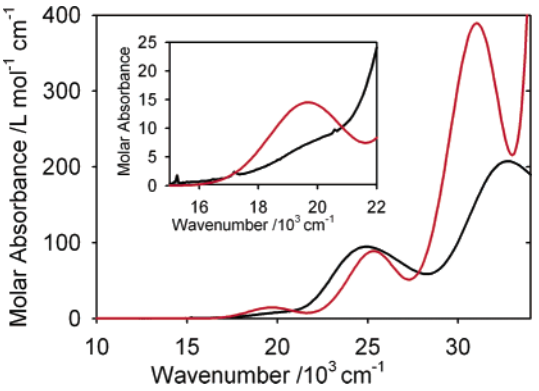

Figure 2. Experimental spectrum (black) of [Ru(DMSO)$_2Cl_2$(opda)] in methanol and calculated TD-DFT (red) electronic spectrum. Inset shows expansion of the data over the weak feature near 19 000 cm^{-1}

no intense visible absorption (Figure 2) since the opda ligand has no low-lying π^* orbitals, and the metal is separated from the ligand by the valence-saturated $-NH_2-$ linkage. The pale yellow compound exhibits three weak transitions below 35 000 cm^{-1} and a somewhat stronger band centered near 40 000 cm^{-1}.

Electrochemical Data. The electrochemical behavior of **1** (Supporting Information Figure S2) is similar to that of [Ru(bpy)$_2$(opda)]$^{2+}$ [72] exhibiting a single irreversible oxidation wave at +0.97 V vs NHE believed to generate a Ru^{III}−bqdi species. Because of its irreversibility it has not been further investigated.

The DMSO ligand in species **1** is quite labile and can be replaced fairly readily by other ligands, such as water, although the products were not isolated. It is also clear that oxidation to bqdi is facile especially when the solution is basic. Thus, it was no surprise to isolate species **2** when species **1** was treated with dilute ammonia in methanol, in the presence of air.

[Ru(NH_3)$_2Cl_2$(bqdi)] (2). Complex **2** is moderately soluble in dimethylformamide (DMF) and dimethyl sulfoxide (DMSO) and sparingly soluble in water and in methanol. It is insoluble in acetonitrile, ethanol, and acetone. At 298 K, solvolysis occurs in water and also in DMF and DMSO. A 10^{-4} M solution is converted to the final solvolyzed product in neutral water after about 6 h and in DMF after about 24 h at 298 K. These processes are greatly speeded up in hot solvents and inhibited in the presence of chloride. The complex is unstable in the presence of dilute acid or base.

X-ray Structure. The [Ru(NH_3)$_2Cl_2$(bqdi)] complex (Figure 1) lies on plane m and the Ru atom has a distorted tetragonal-bipyramidal RuN_4Cl_2 coordination with the equatorial Ru−N distances (av 2.058 Å, Table 3) and chlorine atoms in axial position (av 2.377 Å). The Ru−NH_3 and Ru−Cl bond distances are typical for Ru^{II} species. The Ru−N_{bqdi} distance of 1.969 Å is short in comparison to the Ru−N_{NH3} distance of 2.148 Å. This short Ru−N_{bqdi} distance should be compared with 2.00 Å in [Ru(bqdi)$_3$]$^{2+}$,[74] [Ru(bqdi)$_2$-

(72) Masui, H.; Lever, A. B. P.; Auburn, P. R. *Inorg. Chem.* **1991**, *30*, 2402.
(73) Connelly, N. G.; Geiger, W. E. *Chem. Rev.* **1996**, *96*, 877.
(74) Rusanova, J.; Rusanov, E.; Ebadi, M.; Christendat, D.; Lever, A. B. P. Unpublished work.

Table 3. Selected Bond Distances (Å) and Angles (deg) for $[Ru(NH_3)_2Cl_2(bqdi)]$ (**2**)[a]

Ru1−N1	1.969(3)	N1−Ru1−N1a	78.4(2)
Ru1−N2	2.149(3)	N1−Ru1−N2a	172.9(1)
Ru1−Cl2	2.373(1)	N1−Ru1−N2	94.6(1)
Ru1−Cl1	2.382(1)	N1a−Ru1−N2	172.9(1)
N1−C1	1.330(5)	N2a−Ru1−N2	92.5(2)
C1−C2	1.408(5)	N1−Ru1−Cl2	94.9(1)
C1−C1a	1.457(7)	N2−Ru1−Cl2	85.1(1)
C2−C3	1.358(6)	N1−Ru1−Cl1	94.4(1)
C2−H2	0.91(3)	N2−Ru1−Cl1	86.6(1)
C3−C3a	1.427(8)	Cl2−Ru1−Cl1	168.0(1)
C3−H3	0.87(5)		

[a] There is a plane of symmetry bisecting the bqdi ligand and containing the Ru−Cl bonds.

$(opda)]^{2+}$,[75] and $[Ru(PPh_3)_2Cl_2(bqdi)]$[76] and 2.02 Å in $[Ru(opda)_2(bqdi)]^{2+}$.[77] The Cl−Ru−Cl angle is 168°, and the Cl atoms are pushed away from the bqdi ligand. The C−C distances (Figure 1C) alternate as expected for a quinonoid structure. There is a 3-D H-bonded network with multiple N−H···Cl connections (N1−H1N···Cl1A N1−H1N = 0.81(5)Å, H1N···Cl1A = 2.68(5) Å, N1···Cl1A = 3.412(3) Å, N1−H1N−CL1A = 152(5)°; N2−H21N···Cl1A N2−H21N = 0.85(5) Å, H21N···Cl1A = 2.62(5) Å, N2···Cl1A = 3.457(4) Å, N2−H21N−CL1A = 168(5)°; N2−H23N···Cl2B N2−H23N = 0.86(6) Å, H23N···Cl2B = 2.83(5) Å, N2···Cl2B = 3.323(4) Å, N2−H23N−CL2B = 118(4)°).

Mass Spectra. Electrospray mass spectroscopy reveals the parent ion at 312 *m*/*e* and signals from the successive loss of each ammonia and the two chlorine atoms. The further fragmentation of species **2** is the subject of a separate publication.[30]

Optical Spectrum. Ruthenium complexes with the bqdi ligand usually exhibit a single intense absorption in the visible region because of a Ru 4dπ → bqdi π^* metal-to-ligand charge transfer (MLCT) transition,[1,4−7,12,14] and species **2** is no exception (Figure 4). The energy of this $^1A_1 \rightarrow {}^1A_1$ transition, here termed ^{1}MLCT3, shows little solvatochromism with the band energies lying at 20 100 cm^{-1} in DMF and MeOH and 19 900 cm^{-1} in water. The half bandwidth ($\Delta_{1/2}$) in water (3300 cm^{-1}) is slightly larger than that in DMF (2680 cm^{-1}) or MeOH (3000 cm^{-1}). The transitions are assigned following the analysis below.

There are two very weak and overlapping bands $^1A_1 \rightarrow {}^1B_2, {}^1B_1$ at 10−11 000 cm^{-1} termed ^{1}MLCT1,2 (Figure 4).

Emission. The Stokes shift in emission is approximately 5400 cm^{-1} in the solid state (Figure 5), and the emission band envelope is a mirror image of the absorption spectrum indicative that emission comes from the same state as the absorption. There appear to be two emitting processes with lifetimes at 30 K of 1270 (40%) and 270 ns (60%) which decrease to 950 (35%) and 250 ns (65%) at 100 K. The emission is therefore fluorescence from the ^{1}MLCT3 state and not phosphorescence from a spin-triplet state (^{3}MLCT3),

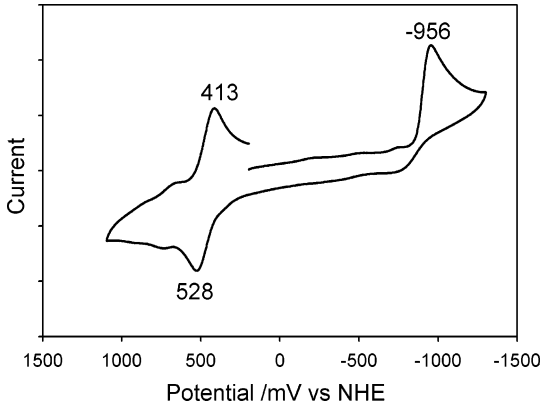

Figure 3. Cyclic voltammogram of $[Ru(NH_3)_2Cl_2(bqdi)]$ (**2**) in dimethylformamide/TBA PF_6, scan rate 100 mV/s. The reference electrode was AgCl/Ag and was corrected to NHE using ferrocene assumed to lie at 0.69 V vs NHE in DMF/TBA PF_6.[73] The small couple, near 0.7 V, just positive of the main redox couple, is absent from voltammograms which are initially scanned to positive potentials and is the result of a coupled chemical process occurring negative of −0.96 V.

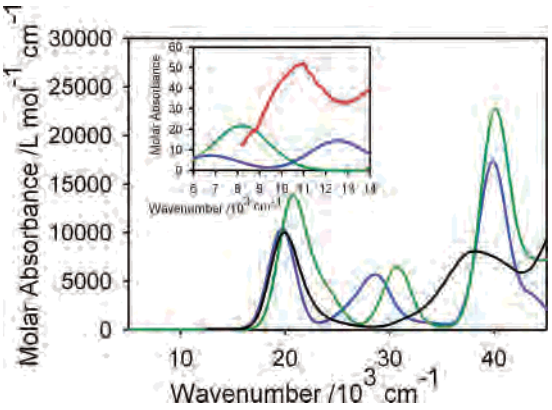

Figure 4. Optical spectroscopic data for $[Ru(NH_3)_2Cl_2(bqdi)]$. Experimental data for species **2** dissolved in water (black). TD-DFT calculated spectra are shown at the B3LYP/Lanl2DZ level in gas phase (blue) and water (PCM) (dark green). The inset shows the weak absorption resulting from ^{1}MLCT1,2.

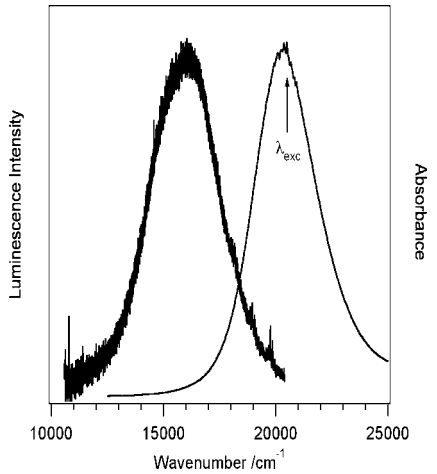

Figure 5. Emission spectrum for $[Ru(NH_3)_2Cl_2(bqdi)]$ in the solid state (left, excitation 488 nm) normalized to the absorption spectrum (right) in DMF solution. The sharp peaks, to the right of the solid-state emission spectrum peak, are resonance-enhanced Raman vibrations.

a conclusion also consistent with the very short lifetime of this state and with the DFT calculations that show that the corresponding spin-triplet state (^{3}MLCT3) lies at much lower

(75) Cheng, H. Y.; Peng, S. M. *Inorg. Chim. Acta* **1990**, *169*, 23.
(76) Venegas-Yazigi, D.; Costamagna, J.; LaTorre, R.; Lever, A. B. P. *Book of Abstracts;* 213th ACS National Meeting, San Francisco, April 13−17, 1997; American Chemical Society: Washington, DC, 1997; p INOR-275.
(77) Milliken, B.; Borer, L.; Russell, J.; Bilich, M.; Olmstead, M. M. *Inorg. Chim. Acta* **2003**, *348*, 212.

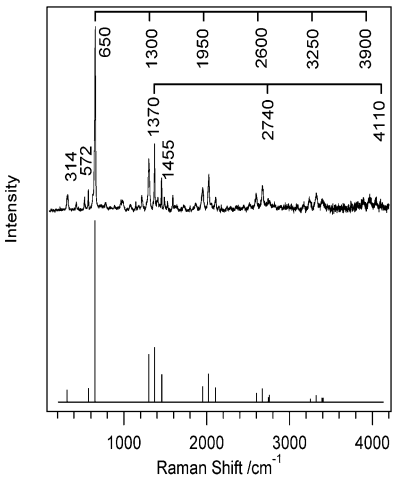

Figure 6. Resonance Raman (RR) spectrum of solid $[Ru(NH_3)_2Cl_2(bqdi)]$ (**2**). The upper trace shows the experimental spectrum with 488 nm excitation. The two main series of overtones are identified. The lower trace shows the calculated relative intensities of the RR transitions calculated according to the details given in the text.

energy (4680 cm^{-1}). This emission apparently disobeys Kasha's rule[78] in that there are several other spin-singlet states (^{1}MLCT1,2) below ^{1}MLCT3 and three triplet states. This is quite unusual for closed-shell Ru^{II}−diimine species which generally emit phosphorescence from a lower-lying spin-triplet state. However the emission quantum yield is very low, <0.1%. Evidently, the MLCT3 excited state surface is incompletely coupled to these lower-lying states because of the symmetry and the large energy difference.

Electrochemical Data. The voltammogram (Figure 3) exhibits a single reversible wave at $E_{1/2} = +0.47$ V vs NHE in DMF (and in DMSO), assigned to the Ru^{III}/Ru^{II} process. At −0.96 V vs NHE, there is an irreversible process assigned to the two-electron reduction to the Ru^{II}−opda species, nominally $[Ru(NH_3)_2Cl_2(opda)]$ (not further studied). In agreement, rotating-disk electrode steady-state measurements (not shown) reveal that the current passing at −0.96 V is twice as large as that at +0.47 V vs NHE.

Resonance Raman (RR). The spectrum (Figure 6) is dominated by low-frequency vibrations, the most intense lying at 655 cm^{-1} (648 cm^{-1} in the low-temperature (78 K) solid-state spectrum). Fingerprint region vibrations around 1200−1400 cm^{-1} are relatively weak compared with the 655 cm^{-1} band providing information about the nature of the excited MLCT state as discussed below. Agreement (Supporting Information, Table S1) between the experimental and calculated (B3LYP/LanL2DZ) vibrational frequencies is excellent. Analysis of these data reveals a progression of overtones at least to $n = 5$ in the 655 cm^{-1} fundamental plus some combination bands built of other fundamentals, especially one at 1370 cm^{-1}. Assignments are shown in Figure 6.

Computation. The optimized geometries of the complexes (**1** and **2**) differ little from the X-ray structures (Figure 1C, Tables 2, 3, S2, and S3). Both TD-DFT and INDO/S (Supporting Information Tables S4 and S5) were used to predict the electronic spectra of **1** and **2** and the TD-DFT simulated spectra are shown in Figures 2 and 4. Previously,[12] we have demonstrated that for ruthenium diimine species, if not many others, TD-DFT and INDO/S give similar electronic structure descriptions and spectroscopic predictions with the latter being obtainable with much less computational effort. These are, of course, gas-phase calculations, but because the complex is not solvatochromic, we achieve excellent agreement between the observed and calculated data. However, both methods predict an extra transition which has no obvious experimental analogue unless we associate it with the weak shoulder seen to higher energy. This is partly a chloride → bqdi π^* LLCT and is placed at low energy in the calculated gas-phase spectrum because the negative charge on the chloride is not stabilized by the solvent molecules and H-bond interactions (Figure 4) (vide infra).

Table 4. Frontier Orbitals of $[Ru(dmso)_2Cl_2(opda)]$ (**1**) and Their Compositions (B3LYP/LanL2DZ gas-phase calculations)

orbital	energy (eV)	% Ru	% Cl	% dmso	% opda
LUMO+6	2.46	0.1	0.0	0.1	99.9
LUMO+5	2.24	11.7	0.1	14.8	73.4
LUMO+4	0.83	48.6	0.9	46.3	4.2
LUMO+3	0.55	67.0	19.4	12.0	1.6
LUMO+2	0.47	43.2	4.0	49.5	3.3
LUMO+1	0.14	0.1	0.0	0.0	99.9
LUMO	0.09	0.0	0.0	0.0	99.9
HOMO	−7.60	88.0	7.6	3.5	0.9
HOMO−1	−7.61	87.2	8.8	3.2	0.8
HOMO−2	−7.72	91.5	0.1	6.1	2.3

Table 5. Frontier Orbitals of $[Ru(NH_3)_2Cl_2(bqdi)]$ and Their Compositions (B3LYP/LanL2DZ level gas-phase calculations)

orbital	E (eV)	Γ^a	% Ru^b	% bqdi	% Cl	% NH_3
LUMO+3	−0.07	b_1	5.1	94.9	0.0	0.0
LUMO+2	−0.10	b_2 σ^*	79.6	7.1	1.6	11.8
LUMO+1	−1.07	a_1 σ^*	61.8	6.0	27.2	4.9
LUMO	−2.89	b_1 π^*	32.5 (33)	61.4	5.7	0.4
HOMO	−5.14	a_2 δ^*	60.6 (58)	20.5	18.3	0.6
HOMO−1	−5.61	b_1 π	33.6 (44)	38.1	27.9	0.4
HOMO−2	−5.93	a_1 σ	86.9 (92)	6.0	4.4	2.6
HOMO−3	−6.45	a_2 δ	1.2 (23)	65.3	33.3	0.2
HOMO−4	−6.90	b_2	3.6	0.7	91.8	3.8
HOMO−5	−6.97	a_1	8.5	0.4	87.6	3.5
HOMO−6	−7.09	b_1	6.3	10.8	82.2	0.7

^{a} Symmetry labels and relationship to the Ru−bqdi plane (yz). ^{b} Data in parentheses are derived from the INDO/S calculations on the DFT-optimized geometry.

The compositions of the frontier orbitals of **1** and **2** in terms of contributions from ruthenium and the ligands are presented in Tables4 and 5 and Figure S3 (Supporting Information). Some comparative data from the INDO/S calculations are also included in Table 5. The overall Ru contributions to the frontier orbitals are similar, as calculated by the two models. Figure 7 displays the frontier orbitals of **2**.

The occupied Ru 4dπ orbitals, HOMO, HOMO−1, and HOMO−2 (Table 5 and Figure 7), are the t_{2g} set in O_h symmetry. In C_{2v} symmetry (the bqdi ligand is in the yz plane), the three d(t_{2g}) orbitals are described as dδ (d_{xy}), dπ (d_{xz}), and dσ ($d_{z^2-y^2}$) and belong to a_2, b_1, and a_1 irreducible

(78) Kasha, M. *Discuss. Faraday Soc.* **1950**, *9*, 14.

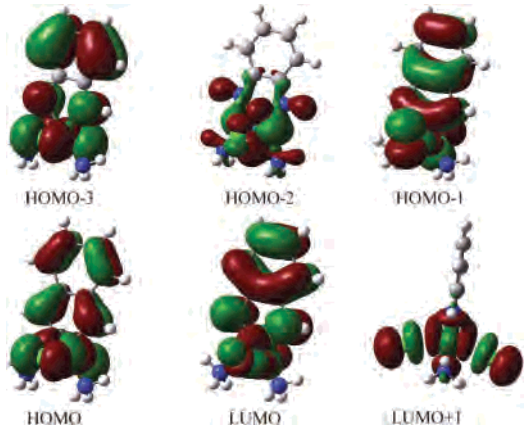

Figure 7. Frontier (B3LYP/LanL2DZ) Kohn−Sham molecular orbitals of species **2**.

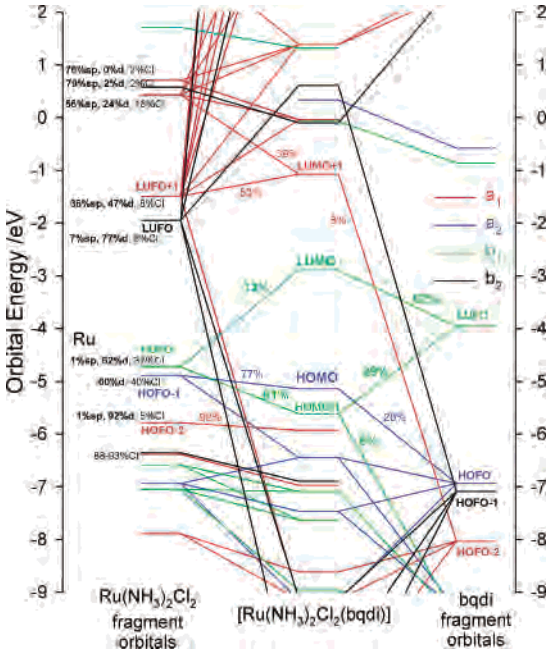

Figure 8. Orbital interaction diagram (B3LYP/LanL2DZ) for $[Ru(NH_3)_2Cl_2(bqdi)]$; $Ru(NH_3)_2Cl_2$ and bqdi are interacting fragments (both in a closed-shell singlet-spin state). Orbitals of a_1, a_2, b_1, and b_2 symmetry are shown in red, blue, green, and black, respectively. Molecular orbitals of the $Ru(NH_3)_2Cl_2$ and bqdi fragments are shifted by 0.7 eV and −0.7 eV, respectively. The MO−FO pairs are connected by lines if the corresponding FO contributions are greater than 5%.

representations, respectively[79,80] (Table 5, Figures7 and 8). The HOMO−2 (dσ) is the purest Ru 4d orbital since it cannot interact with the bqdi ligand π and π* orbitals (no low-energy UFO_{bqdi} of a_1 symmetry for the bqdi ligand, Figure 8), and it also cannot interact effectively with occupied π orbitals of the chloride ligands.

The lowest-unoccupied fragment orbital (LUFO) which is 77% Ru 4dσ* and LUFO+1 (47% Ru 4dσ* and 28% Ru 5s) of the $Ru(NH_3)_2Cl_2$ fragment, and HOFO−1 and HOFO−2 of the bqdi ligand are involved in the ligand-to-metal donation (Figure 8, black and red lines). The three Ru t_{2g} orbitals, being occupied, cannot be involved in metal−bqdi bonding through the ligand-to-metal donation. Instead, the HOFO (61% Ru 4dπ) of the $Ru(NH_3)_2Cl_2$ fragment is involved in covalent bonding with the bqdi ligand via a π-back-bonding interaction with the $LUFO_{bqdi}$ (Figure 8, green lines). The HOFO and the LUFO (i.e., the HOMO and the LUMO of the relevant fragment) are names used to distinguish the fragment molecular orbitals from the molecular orbitals of the complex.

Discussion

First we shall discuss the physical properties of **1** and **2**, and then we will compare the properties of **2** with analogous, less delocalized, systems to show how the extensive delocalization influences the various characteristics of **2**.

$[Ru^{II}(S\text{-}DMSO)_2Cl_2(opda)]$ (1). The experimental and TD-DFT calculated spectra of **1** are shown in Figure 2. The compositions of the frontier MOs are shown in Table 4. Agreement between experimental and calculated transition energies and intensities is excellent (Figure 2). Since the opda ligand is a very poor acceptor, one expects that all the lower lying absorption features are d−d transitions.[80] They would be components of the usual d^6 $^1T_{1g}$ and $^1T_{2g}$ states (in octahedral symmetry) split in the low symmetry of this molecule. Indeed the three weak features ($\epsilon < 100\ M^{-1}\ cm^{-1}$) lying below 35 000 cm^{-1} are d−d components of these orbital triplets. At higher energy, 37 000−45 000 cm^{-1}, there are internal transitions of the opda and DMSO ligands which are not discussed save to note that the calculation also predicts very weak MLCT transitions Ru 4d → opda π* in this region.

$[Ru(NH_3)_2Cl_2(bqdi)]$ (2). The most dramatic result is the 32% Ru 4d character in the LUMO of the complex which is primarily derived from the LUMO of the bqdi ligand (Table 5). The electronic coupling between filled Ru 4dπ and unoccupied bqdi π* orbitals, a measure of π-back-donation, is quite high and exceeds any previously reported (expressed per ligand) values for the Ru−bqdi complexes. It is similar to the extent of orbital mixing in the nitrosyl (NO^+) localized LUMO and LUMO+1 of complexes of electron-rich ruthenium nitrosyl species such as $[Ru(NH_3)_5(NO)]^{3+}$ (25% Ru 4d character in both the LUMO and LUMO+1).[81] The primary intent of this contribution is to discuss how this back-bonding interaction between Ru 4dπ and ligand π and π* influences the various physical properties of this complex.

Electronic Spectra. Complexes of the type $[Ru^{II}L_4Q]$ (where Q is a quinonoid ligand) with a wide variety of L ligands are well-known and commonly yield one intense visible region transition assigned as Ru 4dπ → Q π*.[1,2,5,6,13,72,82−86] In the title species, MLCT3 is primarily

(79) Figgis, B. N.; Hitchman, M. A. *Ligand Field Theory and Its Applications:* Wiley-VCH: New York, 2000.
(80) Lever, A. B. P. *Inorganic Electronic Spectroscopy*; Elsevier Science: Amsterdam, 1984.
(81) Gorelsky, S. I.; da Silva, S. C.; Lever, A. B. P.; Franco, D. W. *Inorg. Chim. Acta* **2000**, *300*−*302*, 698.
(82) Haga, M.; Dodsworth, E. S.; Lever, A. B. P. *Inorg. Chem.* **1986**, *25*, 447.
(83) Da Cunha, C. J.; Dodsworth, E. S.; Monteiro, M. A.; Lever, A. B. P. *Inorg. Chem.* **1999**, *38*, 5399.
(84) Mitra, K. N.; Choudhury, S.; Castineiras, A.; Goswami, S. *J. Chem. Soc., Dalton Trans.* **1998**, 2901.
(85) Das, C.; Kamar, K.; Ghosh, A. K.; Majumdar, P.; Hung, C. H.; Goswami, S. *New J. Chem.* **2002**, *26*, 1409.

Table 6. Experimental and Calculated (TD-DFT) Spectra of $[Ru(NH_3)_2Cl_2(bqdi)]$ (**2**)

obsd ($\times 10^3$ cm^{-1}) (ϵ)[a]	calcd ($\times 10^3$ cm^{-1}) (f)[b,c]	contributing electron excitations[d] and *polarization*
9.8sh[e,f]	8.1 (0.0003)	^{1}MLCT1 HOMO → LUMO (75%) *y*
10.9 (52)[e,f]	12.6 (0.0002)	^{1}MLCT2 HOMO−2 → LUMO (87%) *x*
20.0 (10000)[g,h]	20.5 (0.17)	^{1}MLCT3 HOMO−1 → LUMO (62%) *z*
	24.0 (0.013)	HOMO−3 → LUMO (85%) *y*
31.5 (sh)[g]	27.9 (0.096)	HOMO−6 → LUMO (81%) *z*
38.2 (8100)[g,h]	40.3 (0.23)	HOMO → LUMO+5 (46%) HOMO−1 → LUMO+3 (24%) *z*

[a] Observed in water (molar absorptivity, M^{-1} cm^{-1}). [b] Oscillator strength. [c] The lowest-lying spin-triplet states lie (B3LYP/LanL2DZ) at 2260 (HOMO → LUMO), 4680 (HOMO-1 → LUMO), and 9350 cm^{-1} (HOMO-2 → LUMO). [d] Occupied MO → unoccupied MO (% contribution to the wave function of the excited state). [e] In DMSO. [f] Data in DMF 9.8sh, 10.9(63). [g] Data presented for water, bandwidth $\Delta_{1/2} = 3200$ cm^{-1}, oscillator strength $f = 0.15$. [h] Data in methanol, 20.1 ($\epsilon = 10\,230$, $\Delta_{1/2} = 3000$ cm^{-1}, $f = 0.14$), 37.6br (ϵ=8600). Bandwidths are derived from twice the bandwidth at half-height, measured from the center to the low energy side of the band. The band near 38 000 cm^{-1} is clearly composite so that measurement of bandwidth is not meaningful.

the *z*-polarized excitation HOMO−1 → LUMO (Table 6; a more detailed description of the calculated spectrum is presented in Table S4, Supporting Information). The HOMO−1 and the LUMO are bonding and antibonding combinations of $HOFO_{Ru}$ (Ru 4dπ_{xz}) and $LUFO_{bqdi}$ (π^*) (Figure 8). The overlap population[44] between the metal fragment and the bqdi ligand is 0.031 for HOMO−1 and −0.163 for the LUMO. While one may call the HOMO−1 → LUMO excitation a charge transfer (CT) transition, in fact it is better described as an internal excitation of the Ru(HN−C−C−NH) metallacycle (see RR discussion below). Since it is a transition from the bonding MO to the antibonding MO involving the same pair of metal and ligand fragment orbitals, it is moderately intense, and the intensity of this band is a probe of metal−ligand bonding interactions in complexes.[80,87] The ruthenium CT character for an electron excitation $\phi_i \rightarrow \phi_a$ can be defined[7]

$$\mathrm{CT}\ (\%) = |\%\mathrm{Ru}(\phi_i) - \%\mathrm{Ru}(\phi_a)| \qquad (1)$$

which yields the very small value of 1% for MLCT3.

As noted in Figure 4 and Table 6, there are two other very weak *y*- and *x*-polarized MLCT transitions ($^1A_1 \rightarrow {}^1B_2$, ^{1}MLCT1 and $^1A_1 \rightarrow {}^1B_1$,^{1}MLCT2 respectively) lying at much lower energy than ^{1}MLCT3. These two electric-dipole-allowed transitions originate from the other two d(t_{2g}) orbitals, HOMO (dδ) and HOMO−2 (dσ), to the LUMO. Ruthenium CT characters are 28% for MLCT1 and 54% for MLCT2. However, the low intensities of these MLCT bands originate from the fact that these transitions are polarized in orthogonal directions from the principal component (*z*) of the dipole operator (the *z* axis goes through the Ru atom the center of the bqdi ligand), and the HOMO and HOMO−2 orbital are not coupled with the $LUFO_{bqdi}$.

Magnuson and Taube[88] first discussed the existence of such weak and strong CT transitions in the species $[M^{II}(NH_3)_5(L)]^{2+}$ (M = Ru and Os; L are aromatic nitrogen heterocyclics), presenting a model that is relevant to the Ru^{II}−diimine complex here. While their quantitative interpretation came from an oversimplified MO model in which the energy difference between the weak and strong CT transitions is a result of π-stabilization energy, they correctly described one intense CT transition and two weak CT transitions lying to lower energy as excitations from the M−L bonding and two nonbonding d orbitals, respectively. It turns out that the separation between the weak and strong band is critically dependent on the covalency in the bonds, and the weak band will be too close to the strong band and be obscured except in very delocalized species.[7]

Resonance Raman.[23,89−91] The RR spectrum (Figure 6) collected via excitation into ^{1}MLCT3 (excitation wavelength λ_{exc} 488 nm) shows a very intense band at 655 cm^{-1} which, by comparison with the calculated frequencies and normal modes, is the symmetric $Ru-N_{bqdi}$ stretching vibration within the Ru(NH−C−C−NH) metallacycle and which shows a progression to at least $n = 5$ (Figure 6). The fundamental is resonance enhanced to a much greater degree than the internal C−C and C−N vibrations of the bqdi ligand (Figure 6). The only other mode for which overtones can be clearly identified has a frequency of 1370 cm^{-1}, and corresponding mainly to stretching of the $C{=}N_{bqdi}$ coupled to a ring-breathing bqdi-centered mode and to NH motion (see also Table S1). This is definitive evidence for a significant change in bond coordinates for the metallacycle but much less so for the bqdi ligand itself and is independent experimental evidence that there is very little CT character as far as the bqdi ligand ring in the ^{1}MLCT3 excited state.[1,92,93] The ^{1}MLCT3 transition is then best thought of as an internal $\pi-\pi^*$-type transition within the metallacycle ring (which has quasi-aromatic character[1,72,94]).

The intensity of a given Raman transition is related to the Raman-scattering cross-section, $(\alpha)_{fi}$, between initial state *i* and final state *f*, through eq 2[95−97]

(86) Mitra, K. N.; Choudhury, *S.*; Castiñeiras, A.; Goswami, S. *J. Chem. Soc., Dalton Trans.* **1998**, 2901.
(87) Lever, A. B. P.; Dodsworth, E. S. *Inorganic Electronic Structure and Spectroscopy*; Solomon, E. I., Lever, A. B. P., Eds.; Wiley-Interscience: New York, 1999; Vol. 2, p 227.
(88) Magnuson, R. H.; Taube, H. *J. Am. Chem. Soc.* **1975**, *97*, 5129.
(89) Kincaid, J. R.; Czarnecki, K. In *Comprehensive Coordination Chemistry II*; McCleverty, J. A., Meyer, T. J., Eds.; Elsevier Pergamon: New York, 2003; Vol. 1, p 121.
(90) Reber, C.; Landry-Hum, J. In *Comprehensive Coordination Chemistry II*; McCleverty, J. A., Meyer, T. J., Eds.; Elsevier Pergamon: New York, 2003; Vol. 1, p 559.
(91) Reber, C.; Beaulac, R. In *Comprehensive Coordination Chemistry II*; McCleverty, J. A., Meyer, T. J., Eds.; Elsevier Pergamon: New York, 2003; Vol. 1, p 287.
(92) Lever, A. B. P.; Masui, H.; Metcalfe, R. A.; Stufkens, D. J.; Dodsworth, E. S.; Auburn, P. R. *Coord. Chem. Rev.* **1993**, *93*, 317.
(93) Stufkens, D. J.; Snoeck, T. L.; Lever, A. B. P. *Inorg. Chem.* **1988**, *27*, 953.
(94) Crociani, B.; Boschi, T.; Pietropaolo, R.; Belluco, U. *J. Chem. Soc A* **1970**, 531.
(95) Heller, E. J. *Acc. Chem. Res.* **1981**, *14*, 368.

$$I_{i\rightarrow f} \propto \omega_I \omega_s{}^3(\alpha)_{fi}{}^*(\alpha)_{fi} \quad (2)$$

where ω_I is the frequency of the incident radiation and ω_s is the frequency of the scattered radiation. Scattering cross-sections for RR transitions are easily calculated from Heller's time-dependent theory of spectroscopy

$$(\alpha)_{fi} = \frac{i}{\hbar}\int_0^\infty \langle \phi_f | \phi(t) \rangle \exp\{i(\omega_i + \omega_I)t - \Gamma t\} \mathrm{d}t \quad (3)$$

where $|\phi_f\rangle = \mu|\chi_f\rangle$ is the final vibrational state, $|\chi_f\rangle$, of the ground electronic surface multiplied by the transition moment μ, $|\phi(t)\rangle = \exp(-i\hat{H}_{ex}t/\hbar)|\phi\rangle$ is a moving wave packet propagated by the Hamiltonian on the excited-state potential energy surface, $|\phi\rangle = \mu|\chi_i\rangle$ is the initial vibrational state of the ground electronic state multiplied by the transition dipole, and Γ is a damping factor that leads to the width of each individual vibronic transition. The integral $\langle f_f|\phi(t)\rangle$ is the autocorrelation function and is the key quantity in any time-dependent calculation. The zero-point energy of the ground electronic surface is given by $\hbar\omega_i$.

In the simplest case where (i) harmonic potential energy surfaces are used to represent the ground state and a single-excited state, (ii) the transition dipole moment μ_{if} is constant, and (iii) no mixing occurs between normal coordinates in the excited state, the appropriate autocorrelation function reduces to a closed formula which is then Fourier transformed according to eq 3 to lead to the excitation profile, $I_{i\rightarrow f} = f(\lambda_{exc})$, and therefore to the relative RR intensity at 488 nm. If we further assume identical force constants in both the ground and excited states, the autocorrelation function is given by eq 4[98]

$$\langle \phi|\phi(t)\rangle_s = \prod_k \left\{ \exp\left[-\frac{\Delta_k{}^2}{2}(1 - \exp(-i\omega_k t)) - \frac{i\omega_k t}{2} \right] \times (1 - \exp(-i\omega_k t))^{n_k} \times \frac{(-1)^{n_k}\Delta_k^{n_k}}{(2^{n_k} n_k!)^{1/2}} \right\} \exp(-iE_{00}t) \quad (4)$$

In eq 4, E_{00} is the electronic origin, ω_k and Δ_k are the wavenumber and the (dimensionless) displacement of the kth normal mode, respectively, and n_k is the vibrational quantum number of the kth normal mode in the final vibrational wave function, $|\chi_f\rangle$. For example, in a system with only two modes, α and β, for the final state corresponding to the first overtone of α, $n_\alpha = 2$ and $n_\beta = 0$; for the final state corresponding to the combination band $\alpha + 2\beta$, $n_\alpha = 1$, and $n_\beta = 2$. All frequencies and energy parameters in the above equations are given per inverse centimeter.

All vibrational frequencies were determined experimentally from the Raman spectrum. The energy of the electronic origin, E_{00}, was determined from the absorption and luminescence spectra. The most important adjustable parameters are the offsets, Δ_κ (dimensionless units), of the potential energy minima along each normal coordinate. For harmonic potential energy surfaces, as used here, the sign of each Δ_κ cannot be determined and throughout the following, only absolute values of Δ_κ are given. It is obvious from the RR spectrum that the 655 cm^{-1} mode has the largest offset Δ, as its resonance enhancement is largest. We include 5 modes, sufficient to reproduce most overtone and combination bands. The DFT calculations identify 12 totally symmetric normal modes involving the bqdi ligand and the ruthenium center. Including all modes in the calculations is possible, but does not significantly improve the agreement between the experimental RR spectrum and the calculated intensities. The offsets, Δ, for all totally symmetric normal coordinates not included in Table 7 are less than 0.05. The damping factor was set to a high enough value to obtain smooth calculated intensity profiles but to a sufficiently low value to be sure that the initial dynamic of the system was not totally dependent on the damping. Calculated RR intensities are compared to the experimental spectrum in Figure 6b. The agreement is very good, in view of the simplifications inherent to the model used. The model is appropriate because the absorption bands shown in Figures5 and 9 are well separated from intense bands higher in energy. Numerical values for all offsets, Δ_κ, and all other parameters used for the calculations are summarized in Table 7.

Table 7. Parameters for the Calculation of the Resonance Raman Intensities in Figure 6

quantity	energy (cm^{-1})	offset Δ (dimensionless units)
mode 1	314	1.2
mode 2	572	0.7
mode 3	650	2.33
mode 4	1370	0.6
mode 5	1456	0.4
E_{00}	16500	na
Γ^a	1000	na

[a] Damping factor, see eq 3.

The potential energy surfaces defined by the analysis of the RR intensities can be used to calculate the luminescence and absorption spectra, and Figure 9 demonstrates that the agreement between calculated and experimental spectra is exceptionally good. The luminescence spectrum narrows down the range for the energy of the electronic origin, E_{00}, more so than the RR intensities, but the lack of vibronic structure in the luminescence spectrum prevents an identification of individual offsets, Δ, along any normal coordinate.

The offsets determined from the RR intensities lead to an absorption bandwidth in excellent agreement with the experimental spectrum. Note that the origin for the calculated absorption spectrum in Figure 9 is shifted to higher energy by approximately 1500 cm^{-1} than that for the luminescence and RR calculations, but it is still well within the region of overlap between the absorption and luminescence spectra of Figure 5. The largest offsets Δ in Table 7 are observed along the normal coordinate with a frequency of 650 cm^{-1} and the normal coordinate with a frequency of 1370 cm^{-1}. These mode frequencies with the largest offsets, Δ, are similar to the extensively studied lowest-energy MLCT excited state

(96) Zink, J. I.; Shin, K.-S. K. *Adv. Photochem.* **1991**, *16*, 119.
(97) Wexler, D.; Zink, J. I.; Tutt, L. W.; Lunt, S. R. *J. Phys. Chem.* **1993**, *97*, 13563.
(98) Tannor, D. J.; Heller, E. J. *J. Chem. Phys.* **1982**, *77*, 202.

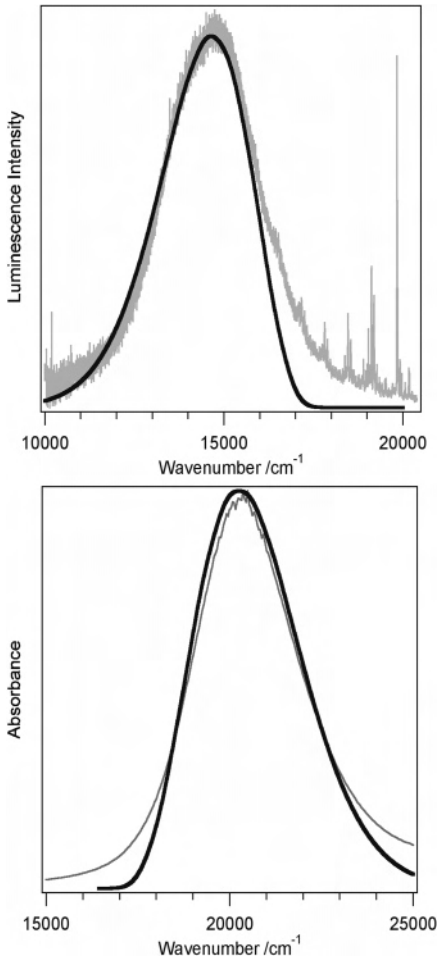

Figure 9. (upper) Experimental emission (gray) and calculated emission (solid black) of **2**. (lower) Experimental absorption band (gray) and calculated absorption (solid black) of **2** in DMF solution.

in $[Ru(bpy)_3]^{2+}$, where the luminescence band shapes and RR intensities have been analyzed with offsets along two normal coordinates with frequencies of 400 and 1380 cm^{-1}, respectively, leading to offsets, Δ, of 1.4 and 1.5, respectively,[99−102] in contrast to the title compound, where the two largest offsets are 2.33 and 0.60, a variation by a factor of 4. This simple comparison illustrates the fundamentally different electronic structure of **2** compared to complexes with polypyridine ligand systems.

The DFT-calculated normal modes provide additional information. One of the totally symmetric modes is calculated at 662 cm^{-1}, close to the experimental frequency of 650 cm^{-1}, and it is predominantly a Ru−N_{bqdi} stretching motion in the Ru−bqdi plane. Such motion is difficult for polypyridine ligands. This mode involves the Ru center, and an offset along its normal coordinate does not correspond to a large transfer of electron density onto the ligand. A second, totally symmetric mode with a calculated frequency of 1392 cm^{-1} (corresponds with the experimental 1370 cm^{-1} band) shows a large resonance enhancement. It involves predominantly N═C stretching causing a breathing motion in the metallacycle in the *yz* plane and is strongly coupled to a breathing motion of the bqdi ligand. These characteristics can be compared to the offsets. The orbital population change, following the ^{1}MLCT3 transition, leads to a weakening of the Ru−N_{bqdi} bonds, which has to be coupled with a $NCCN_{bqdi}$ bending deformation to keep the appropriate structure of the complex. The mode at 662 cm^{-1} incorporates both of these characteristics, and its large resonance enhancement can therefore be rationalized from the DFT calculations. HOMO−1 is bonding with respect to the Ru−N_{bqdi} bond, while the LUMO is antibonding with respect to this bond. This large change in bonding character would lead to a significant resonance enhancement of this mode, as is observed. Qualitatively, the RR intensities therefore correspond to the picture derived from the DFT calculations. The last large offset and resonance enhancement occurs along the mode observed at 314 cm^{-1}. Its frequency corresponds closely to the mode calculated at 317 cm^{-1}, which involves predominantly Ru−NH_3 stretching, coupled weakly into breathing in the metallacycle ring. The Ru−NH_3 bond elongation is expected from the MO plots in Figure 7. The HOMO−1 is nonbonding along the Ru−NH_3 bond axis, the LUMO has significantly more antibonding character and longer Ru−NH_3 bonds are expected, in particular, in the absence of significant electron loss at the metal center, which could lead to a decrease of the bond length because of stronger electrostatic attraction.

There is substantial geometric distortion of the ^{1}MLCT3 excited state, relative to the ground state, as shown by the long progression in the Ru−N_{bqdi} mode frequency. The reorganization energy associated with this distortion can be estimated from a sum over all vibrational frequencies (in wavenumbers) multiplied by the square of the dimensionless offset

$$\chi = {}^1/_2 \sum \text{frequency} \times (\text{offset})^2 \qquad (5)$$

Using the frequencies in Table 7, this yields a value of ~2500 cm^{-1}. To a zero-order approximation, ignoring, inter alia, configurational interaction and assuming that the outer-sphere reorganization energy, χ_o, cancels out,[87] the difference between the absorption maximum of ^{1}MLCT3 (20 100 cm^{-1}), and the E_{oo} energy of emission (16 500 cm^{-1}, Table 7), *in the frozen state*, is the inner-sphere reorganization energy χ_i(MLCT3). Using this approximation, an upper estimate of χ_i(MLCT3) is 3600 cm^{-1}. However χ_i(MLCT3) calculated at the B3LYP/TZVP level (vide infra) is 1200 cm^{-1}, probably a more accurate estimate than the above spectroscopically derived χ_i values.

Impact of this Extensive Delocalization and Comparison with Related Species. To understand how the properties of **2** reflect the extensive delocalization, we compare data with the corresponding properties of related bqdi species (Table 8). The species with the least π-back-donation to bqdi should be the triphenylphosphine species **7**, **8**, and **9** and also species **5** since the PPh_3 and bpy compete with the bqdi ligand for Ru 4dπ electron density. The tetrammine **3** and

(99) Dallinger, R. F.; Woodruff, W. H. *J. Am. Chem. Soc.* **1979**, *101*, 4391.
(100) Krausz, E.; Ferguson, J. *Prog. Inorg. Chem.* **1989**, *37*, 293.
(101) Kumar, C. V.; Barton, J. K.; Gould, I. R.; Turro, N. J.; Van Houtens, J. *Inorg. Chem.* **1988**, *27*, 648.
(102) Kalyanasundaram, K. *Coord. Chem. Rev.* **1982**, *46*, 159.

Table 8. Comparative Structural and Electrochemical Information for Ru^{II}−bqdi Species

complex[j]	*d*(Ru−N) (Å) x-ray	*d*(Ru−N) (Å) B3LYP	*d*(C═N)[b] (Å) x-ray	*d*(C−C)[c] (Å) x-ray	$E_{1/2}$[$Ru^{III/II}$] and [(bqdi)/bqdi$^-$)] (V vs NHE)		E_L(bqdi) (V vs NHE)[d]
(**2**) $[Ru(NH_3)_2Cl_2(bqdi)]$	1.97	1.99	1.33	1.46	0.47	−0.96[i]	0.41
(**3**) $[Ru(NH_3)_4(bqdi)]^{2+}$	na[a]	2.04	n.a.	n.a.	1.1	−0.63[i]	0.41
(**4**) $[Ru(opda)_2(bqdi)]^{2+}$	2.02	2.03	1.35	1.43	na	na	na
(**5**) $[Ru(bpy)_2(bqdi)]^{2+}$	2.02	2.04	1.35	1.43	1.59	−0.23	0.28
(**6**) $[Ru(acac)_2(bqdi)]$	1.96	1.99	1.32	1.45	0.55[e]	−0.96[e]	0.43
(**7**) $[Ru(PPh_3)_2Cl_2(bqdi)]$[d]	1.98	nc[f]	1.32	1.43	0.91	−0.70	0.30
(**8**) $[Ru(PPh_3)_2(CH_3CN)_2(bqdi)]^{2+}$[d]	2.01	nc[f]	1.31	1.46	1.89	−0.24	0.21
(**9**) $[Ru(PPh_3)_2(CH_3CN)Cl(bqdi)]^{+}$[d]	1.97,2.01	nc[f]	1.32	1.46	1.42	−0.41	0.27

[a] Not available. [b] *d*(C═N) from the B3LYP/LanL2DZ calculations was 1.34−1.35 Å. [c] Between the two exocyclic C═NH. [d] Data from refs 8, 76, and 103−105. [e] Measured in this laboratory. [f] Not calculated. [i] Irreversible. [j] opda = *o*-phenylenediamine, acac = acetylacetone.

bis-opda **4** species would be the next in sequence because these neutral co-ligands are good bases and have no π-accepting character. The acetylacetone species **6** may well be comparable to species **2** because the co-ligand is anionic and not a good π acceptor. This sequence is reflected qualitatively in a number of features. Specifically the Ru−N_{bqdi} bonds of species **3**, **4**, and **5** are all longer than those of species **2** and **6**. The C═N_{bqdi} bond is obviously less sensitive to the electronic nature of the co-ligand, but the C−C bond connecting the two exocyclic C═N_{bqdi} bonds does appear slightly shorter in species **4** and **5** than in **2** and **6**.

Electrochemical Properties. The reduction potential at the bqdi ligand is very sensitive to these co-ligands and varies dramatically in the fashion expected (i.e., shifting to more negative potentials as π-back-donation to bqdi increases). The reduction potentials of bound ligands can be correlated[106] with the sum of the ligand electrochemical parameters[15,16,107] of the co-ligands. The slope of such a correlation of $E_{1/2}$(L/L$^-$) versus $\sum E_L$(L) is a measure of the sensitivity of the bound ligand to the co-ligands. For Ru−bipyridine and Ru−bipyrazine reduction, the slopes are 0.25 and 0.33, respectively. For the series $[RuWXYZ(bqdi)]^{n+}$ illustrated in Figure 10 (includes some additional complexes as cited) the slope is 0.45 ± 0.03 showing the greater sensitivity of the bqdi ligand, but evidently it is not as sensitive the Ru−NO^+ species (slope 0.62 ± 0.04).[106]

***E*$_L$ Parameter.** Ligand electrochemical parameter (E_L(L)) theory was developed[15,16,87,106,107,109] not only to provide a means to predict and assign electrochemical potentials but also to learn more of the bonding characteristics of a ligand. Good donor ligands have small or negative values of E_L, while good acceptors have high positive values. Normally E_L(L) is a constant, independent of the metal ion to which L is attached and independent of other ligands attached to the same metal ion. This independence, however, can be expected to break down with so-called "noninnocent" ligands whose electron density can be greatly influenced by the metal ion and co-ligands. This is certainly the case for bqdi. Thus, E_L(bqdi) is a variable and should increase with increasing π-back-donation from the metal to bqdi. This is seen (Table 8) to be the case, where E_L(bqdi) varies from 0.28 to 0.42 V (vs NHE). The E_L(bqdi) value generally increases, albeit not linearly, with decreasing Ru−N_{bqdi} distance and increasing % Ru in the LUMO (i.e., with increasing bqdi ← Ru^{II} π-back-donation).

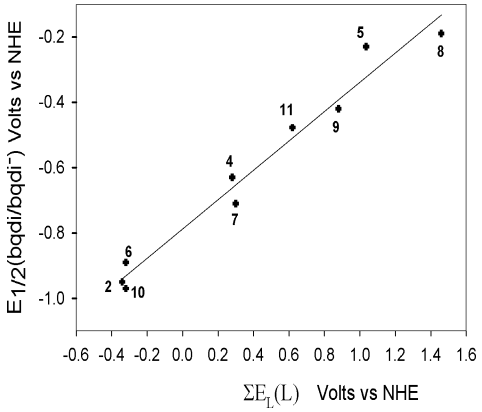

Figure 10. Reduction potential of bound bqdi vs the sum of the ligand electrochemical parameters for the remaining ligands in $[Ru(WXYZ)(bqdi)]^{n+}$. The figure shows the data for the complexes in Table 8 and $[Ru(dtc)_2(bqdi)]$ (**10**) and $[Ru(PPh_3)_2(dtc)(bqdi)]^+$ (**11**)[8,76,104,108] (dtc = diethyldithiocarbamate); reduction of species **2** is irreversible.

Electronic Spectra−Electrochemistry Synergism. The significant Ru−bqdi covalency in $[Ru(NH_3)_2Cl_2(bqdi)]$ reveals itself in a variety of ways, which we will now explore. The energy of a MLCT transition $h\nu$(MLCT) which corresponds to the process $M^{II}L \rightarrow M^{III}L^-$ is related to ΔE(redox) defined as the difference, in this example, between the oxidation potential of the metal $M^{III/II}$[L] and the reduction potential of the ligand L/L$^-$[M^{II}] in the complex concerned.[16,80]

This relationship can be written as

$$h\nu(\text{MLCT}) = [\chi_i + \Delta E(\text{redox}) + \Delta\Delta G_s + Q] + \chi_o + \Delta(\text{sol}) \quad (6a)$$

$$= \Delta E(\text{redox}) + C \quad (6b)$$

where χ_i and χ_o are the inner- and outer-sphere reorganization energies respectively, Δ(sol) is the difference in solvation free energy between the relaxed excited state and the ground state, and $\Delta\Delta G_s = [2\Delta G^\circ_s - \Delta G^\circ_s{}^+ - \Delta G^\circ_s{}^-]$ (difference

(103) Venegas-Yazigi, D. Ph.D. Thesis, Universidad de Chile, Santiago, Chile, 2001.
(104) Venegas-Yazigi, D.; Lever, A. B. P. Unpublished work.
(105) Venegas-Yazigi, D.; Campos-Vallette, M.; Lever, A. B. P.; Costamagna, J.; LaTorre, R. O.; Hernandez, G. W. *J. Chilean Chem. Soc.* **2003**, *48*, 79.
(106) Dodsworth, E. S.; Vlcek, A. A.; Lever, A. B. P. *Inorg. Chem.* **1994**, *33*, 1045.
(107) Vlcek, A. A.; Dodsworth, E. S.; Pietro, W. J.; Lever, A. B. P. *Inorg. Chem.* **1995**, *34*, 1906.

Table 9. Collection of Optical and Electrochemical Data and INDO/S-Calculated Coulomb (J) and Exchange (K) Integrals[a]

complex	$h\nu$(MLCT) (eV)	ΔE(redox) (V)	C (V)	^{1}MLCT3−^{1}MLCT2 (eV) exptl	$K\pi$ ($J\pi$)[a] ($\times 10^3$ cm^{-1})	$K\delta$ ($J\delta$)[a] ($\times 10^3$ cm^{-1})	$K\sigma$ ($J\sigma$)[a] ($\times 10^3$ cm^{-1})
(**2**) [Ru(NH$_3$)$_2$Cl$_2$(bqdi)]	2.50	>1.39	~1.1	1.12	9.1 (39.1)	4.0 (40.2)	1.5 (40.1)
(**3**) [Ru(NH$_3$)$_4$(bqdi)]$^{2+}$	2.64	1.73	0.91	1.35	7.5 (37.6)	3.6 (37.6)	0.74 (35.0)
(**4**) [Ru(opda)$_2$(bqdi)]$^{2+}$	2.62	na	na	1.4 (calcd)	8.2 (38.2)	3.6 (38.0)	0.90 (35.6)
(**5**) [Ru(bpy)$_2$(bqdi)]$^{2+}$	2.41	1.82	0.59	0.76	7.3 (36.4)	2.8 (36.3)	0.7 (32.9)
(**6**) [Ru(acac)$_2$(bqdi)]	2.48	1.51	0.97	1.17	8.7 (38.4)	3.1 (40.2)	1.7 (39.6)

[a] The K and J values for the Ru 4d$_i$ → LUMO transitions, $i = \sigma(d_{z2-y2})$, $\delta(d_{xy})$, $\pi(d_{xz})$. [b] na = not available since oxidation yields the [Ru(opda)(bqdi)$_2$]$^{2+}$ species and not a Ru^{III} species.

between twice the ground state and the oxidized and reduced species free energies of solvation).[80,110]

The parameter Q (eq 6a) is defined as the energy of the process (using our example)

$$[M^{II}L]^- + [M^{III}L]^+ \rightarrow M^{II}L + [M^{III}L^-] \qquad (7)$$

which involves the gas-phase electron transfer of an electron from the singly reduced ground state species to the singly oxidized ground state species, to generate, on the right, the ground state and the thermally equilibrated excited state.

There is the implicit assumption for eq 6a that the MOs involved in the CT transition and the electrochemical redox processes are the same. For the reduction of [Ru^{II}(NH$_3$)$_2$Cl$_2$(bqdi)], this assumption is valid: an electron is added to the LUMO in both reduction and CT transition. However, upon oxidation of [Ru^{II}(NH$_3$)$_2$Cl$_2$(bqdi)], the electron is removed from the HOMO of the complex (i.e., not the same orbital (HOMO−1) that is involved in the principal MLCT transition at 21 000 cm^{-1}). In this situation any desired factorization of eq 6a would require the relevant d−d splitting to be taken into account.

The eq 6a is commonly reduced to eq 6b, and term C is commonly found to be positive but small when one is concerned with the intense allowed CT band in the visible region of, for example, Ru^{II} polypyridine and diimine species; generally, the value of C is close to 0.2 eV.[5,7,110] Indeed the initial assessment[110] of eq 6a involved 33 ruthenium polypyridine complexes which yielded $C = 0.21 \pm 0.11$ eV.[82] Significant deviations from this relationship occur[5,16] when there is extensive coupling between the metal and the diimine ligand, bqdi in this case (Table 9).

Magnuson and Taube[88] assumed that the metal dπ orbital was stabilized by interaction with the ligand π^*-based LUMO and was the most stabilized of the d(t$_{2g}$) set, such that the transition therefrom has the highest energy. In the case of [Ru^{II}(NH$_3$)$_2$Cl$_2$(bqdi)], the Ru 4dπ orbital is not the lowest-energy orbital of the three occupied 4d orbitals (Table 5). Moreover, the DFT-calculated separation between 4dδ and 4dπ within the split Ru 4d(t$_{2g}$) set is 0.47 eV (3800 cm^{-1}), while the separation between ^{1}MLCT1 and ^{1}MLCT3 is 10 000 cm^{-1} (exptl) or 12 400 cm^{-1} (TD-DFT). However, the key issue in the assessment of MLCT energies of the Ru^{II}−diimine complexes is not the t$_{2g}$ orbital splitting but

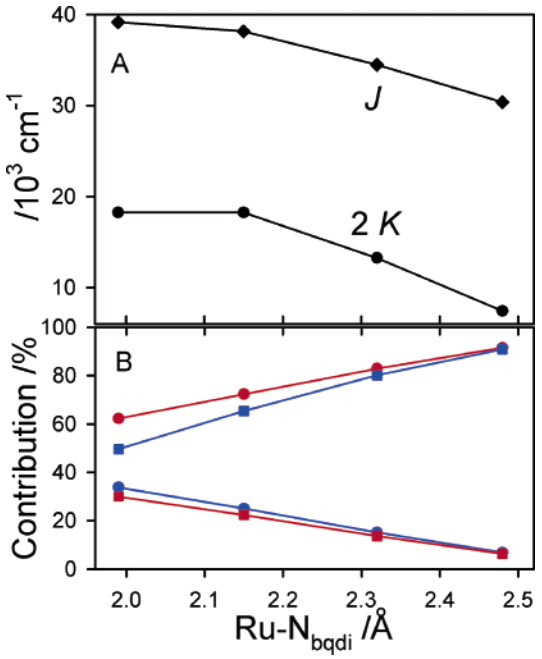

Figure 11. (A) Magnitude of Coulomb (diamonds) and exchange (circles) integrals (INDO/S) for the transitions between the Ru 4d$_{xz}$ + bqdi π^* and Ru 4d$_{xz}$ − bqdi π^* MOs of [Ru^{II}(NH$_3$)$_2$Cl$_2$(bqdi)] as a function of the Ru−N$_{bqdi}$ distance and (B) the mixing of the corresponding fragment orbitals: Ru 4d$_{xz}$ (red lines) and bqdi π^* (blue lines) for the occupied Ru 4d$_{xz}$ + bqdi π^* MO (squares) and unoccupied Ru 4d$_{xz}$ − bqdi π^* MO (circles).

the magnitude of the exchange integrals (K) between the relevant occupied and unoccupied MOs. These integrals depend on the nature of the donor orbital from which the electron is promoted to the acceptor orbital which, in the case of the Ru^{II}-bqdi species, is the LUMO.

To zero order (i.e., no configurational interaction) within the Hartree−Fock model, the energy of a one-electron spin-allowed transition in a molecule with a closed-shell singlet configuration is given by eq 8[80,111]

$$h\nu(\phi_i \rightarrow \phi_a) = \epsilon_a - \epsilon_i - J(i,a) + 2K(i,a) \qquad (8)$$

(i.e., the difference in MO energies concerned ($\epsilon_a - \epsilon_i$) is corrected by the factor ($-J + 2K$) where J and K are the Coulomb and exchange integrals between the MOs i and a)-.[80] Table 9 lists the J and K values for three d(t$_{2g}$) → LUMO electron excitations. The Coulomb integrals are not especially sensitive to the Ru 4dπ−bqdi π^* mixing (Figure 11). On the other hand, $K(i, a)$ varies significantly with the symmetry

(108) Venegas-Yazigi, D.; Mirza, H.; Lever, A. B. P.; Lough, A. J.; Costamagna, J.; LaTorre, R. *Acta Crystallogr.* **2000**, *C56*, e247.
(109) Fielder, S. S.; Osborne, M. C.; Pietro, W. J.; Lever, A. B. P. *J. Am. Chem. Soc.* **1995**, *117*, 6990.
(110) Dodsworth, E. S.; Lever, A. B. P. *Chem. Phys. Lett.* **1986**, *124*, 152.
(111) Gorelsky, S. I. In *Comprehensive Coordination Chemistry II*; McCleverty, J. A., Meyer, T. J., Eds.; Elsevier Pergamon: New York, 2003; Vol. 2, Chapter 2.38, p 467.

Table 10. Molar Absorbance (ϵ), Bandwidth ($\Delta_{1/2}$), and Oscillator Strength (f) for ^{1}MLCT3

complex	solvent	$h\nu$ ($\times 10^3$ cm^{-1}) (ϵ)	$\Delta_{1/2}$ ($\times 10^3$ cm^{-1})	f^b	ref
(**2**) $[Ru(NH_3)_2Cl_2(bqdi)]$	MeOH[a]	20.1 (10 200)	3.0	0.14	this work
(**3**) $[Ru(NH_3)_4(bqdi)]^{2+}$	0.1 M aq H_3PO_4	21.3 (10 200)	3.6	0.17	4
(**4**) $[Ru(opda)_2(bqdi)]^{2+}$	DMF	21.1 (4890)	3.6[c]	0.08	77
(**5**) $[Ru(bpy)_2(bqdi)]^{2+}$	CH_3CN	19.4 (17 400)	2.6	0.21	72
(**6**) $[Ru(acac)_2(bqdi)]$	MeOH	19.9 (16 400)[c]	2.8[c]	0.21	86

[a] For other solvents see footnotes to Table 6. [b] Oscillator strengths were evaluated using $f = 4.6 \times 10^{-9} \times \epsilon \times \Delta_{1/2}$. [c] Data measured on samples in our laboratory.

of the donor orbital *i* and particularly with the contribution of the corresponding Ru 4d orbital to the LUMO, which is zero for the dσ and dδ but is very significant for dπ (Table 9 and Figure 11). This variation is related[5,6,7,12,14,26,112,113] to the fact that where the CT transition involves the bonding and antibonding combinations of the same FO pair, the electron distribution in the excited state is close to that in the ground state and the CT distance (measured via the Stark effect[114−116]) differs from the apparent geometric distance between metal and ligand centers. The Coulomb integrals depend inversely on the donor−acceptor separation. As illustrated in Figure 11A, their values also increase with increasing metal−ligand coupling, but the magnitude of this increase is much less than for corresponding exchange integrals. In the case of $[Ru^{II}(NH_3)_2Cl_2(bqdi)]$, when the Ru−bqdi distance is increased from the equilibrium Ru−N_{bqdi} distance of 1.99 to 2.5 Å, the *J*(HOMO−1, LUMO) decreases by 25%, while the corresponding exchange integral *K*(HOMO−1, LUMO) decreases by a factor of 2.5 from 9130 cm^{-1} (Table 9) to 3720 cm^{-1} (Figure 11A). Thus, the magnitude of *K* reflects the metal−ligand covalency or, in the case of the Ru−bqdi species, the bqdi ← Ru^{II} π-back-donation component of the metal−ligand bond. The *K*(HOMO−1, LUMO) value for $[Ru^{II}(NH_3)_2Cl_2(bqdi)]$ is the highest Ru 4dπ−L π* value we have yet recorded on an experimentally known species. This is obviously associated with the strong π-back-donating interaction that results in a 32% Ru 4dπ contribution to the LUMO. Note for comparison that the corresponding *K*(Ru dπ,LUMO) values for $[Ru(bpy)_3]^{2+}$ (^{1}E MLCT) and $[Ru(NH_3)_4(bpy)]^{2+}$ (intense visible region MLCT) are 1460 and 4160 cm^{-1}, respectively.[6]

Most researchers focus only on the most intense MLCT transition (^{1}MLCT3). The less intense ^{1}MLCT1,2 transitions can be analyzed in the same fashion. For these transitions in the title compound, *C* is −0.13 eV for ^{1}MLCT1 and ∼0 eV for ^{1}MLCT2, similar to the value for the corresponding weak MLCT band in $[Ru(bpy)_2(bqdi)]^{2+}$.[16] For the two excited states arising from the weak and strong MLCT transitions at 10 900 and 20 100 cm^{-1}, respectively, the solvation contributions and the outer-sphere reorganization energy terms will be similar for both excited states.

The inner-sphere reorganization energies for the MLCT states will vary since MLCT3 involves an excitation of an electron from the Ru−bqdi bonding HOMO−1 to the antibonding LUMO while the MLCT1,2 transitions involve excitations from the nonbonding/weakly antibonding orbitals (the HOMO and HOMO−2). The analysis of the RR data (Table 7) yields ∼2500 cm^{-1} as an estimate for χ_i (MLCT3). According to the B3LYP/TZVP calculations, the χ_i values are 1200 cm^{-1} for MLCT3, 1060 cm^{-1} for MLCT1, and 880 cm^{-1} for MLCT2.[117] Since these values are positive, they cannot contribute to making *C* zero or negative (eq 6a). Thus the major difference likely lies in the magnitude of *Q* (eqs 6a). The detailed analysis of terms in eq 6 is a subject of the separate publication.[117]

Oscillator Strengths. Table 10 reports molar absorbance, bandwidth, and oscillator strength data of the principal visible region band (^{1}MLCT3) for the compounds to be compared. The somewhat broader bandwidths of species **3** and **4** probably reflect inclusion of the higher-frequency internal bqdi vibrational frequencies since these species involve greater charge transfer than species **2** and **6**. The increased bandwidth for species **2** in water (Table 6) is likely a consequence of the inclusion of high-frequency N−H···O vibrations due to H-bonding. There is no significant trend in oscillator strengths aside from the larger values seen for compounds **3**, **5**, and **6**. For species **3**, this may be the result of a significant solvent effect in the acidic medium. Compound **5** has a significantly more intense ^{1}MLCT3 but may be atypical because of mixing of bipyridine and bqdi orbitals.

Analysis of Chemical Bonding between the Metal and the bqdi Ligand. The chemical bonding between the metal and the bqdi ligand in complex **2** can be described in terms of donation from the bqdi ligand to the metal fragment ($Ru^{II}(NH_3)_2Cl_2$) and π-back-donation from the metal fragment to the bqdi ligand. Moreover, it is possible to factorize these orbital interactions into different irreducible representations (a_1, a_2, b_1, and b_2 for complexes with C_{2v} symmetry). One may calculate the following contributions for each occupied molecular orbital of the complex: (i) charge donation through the mixing of the occupied orbitals of the bqdi fragment and the unoccupied orbitals of the metal fragment (this donation can be further split into σ and π donation), (ii) charge π-back-donation through the mixing of the occupied orbitals of the metal fragment and the

(112) Shin, Y. G. K.; Brunschwig, B. S.; Creutz, C.; Newton, M. D.; Sutin, N. *J. Phys. Chem.* **1996**, *100*, 1104.
(113) Endicott, J. F.; Schlegel, H. B.; Uddin, M. J.; Seniveratne, D. S. *Coord. Chem. Rev.* **2002**, *229*, 95.
(114) Oh, D. H.; Sano, M.; Boxer, S. G. *J. Am. Chem. Soc.* **1991**, *113*, 6880.
(115) Bublitz, G. U.; Laidlaw, W. M.; Denning, R. G.; Boxer, S. G. *J. Am. Chem. Soc.* **1998**, *120*, 6068.
(116) Walters, K. In *Comprehensive Coordination Chemistry II*; McCleverty, J. A., Meyer, T. J., Eds.; Elsevier Pergamon: New York, 2003; Vol. 2, p 303.
(117) Gorelsky, S. I.; Lever, A. B. P. Unpublished work.

Table 11. Net Charge of the bqdi Ligand, Metal-to-bqdi π-back-donation, and RuL−bqdi and Ru−N_{bqdi} Bond Orders in the $[Ru^{II}(L)_x(bqdi)]$ Complexes (gas-phase B3LYP/LanL2DZ calculations)

complex	q_{bqdi}[a] (au)	CT_b[b] (au)	% Ru (% Ru 4d) in LUMO	% $HOFO_{Ru}$ in LUMO	% $LUFO_{bqdi}$ in LUMO	bond order RuL−bqdi (Ru−N_{bqdi})[e]
(**2**) $[Ru(NH_3)_2Cl_2(bqdi)]$	−0.14	0.72	32.5 (31.9)	32.7	61.7	2.22 (0.76)
(**6**) $[Ru(acac)_2(bqdi)]$	−0.12	0.72	31.5 (31.1)	35.0	61.7	2.21 (0.77)
(**5**) $[Ru(bpy)_2(bqdi)]^{2+}$	0.18	0.39	18.4 (17.9)	19.2	74.6	1.80 (0.61)
(**4**) $[Ru(opda)_2(bqdi)]$	0.22	0.41	22.5 (21.0)	12.9+7.8[c]	72.5	1.91 (0.70)
(**3**) $[Ru(NH_3)_4(bqdi)]^{2+}$	0.25	0.38	20.7 (19.5)	20.0	73.9	1.85 (0.69)
(**12**) $[Ru(NH_3)_5(NO)]^{3+}$	0.24	0.96[d]	25.4 (24.2)	22.2[d]	73.0[d]	1.76

[a] The MPA charge of the bqdi ligand or the NO ligand (in the case of $[Ru(NH_3)_5(NO)]^{3+}$). [b] CT_b = π-back-donation from the Ru fragment to bqdi (or NO^+) as derived from the $LUFO_{bqdi}$ occupancy in the complex; for $[Ru(NH_3)_5(NO)]^{3+}$, both the LUMO and LUMO+1 should included be included in calculating π-back-donation. [c] Contribution from $HOFO-5_{Ru}$. [d] The Ru-to-NO^+ π-back-donation involves two degenerate orbitals: LUMO+0,1 of the NO^+ ligand and HOMO−1,2 of the $Ru(NH_3)_5^{3+}$ fragment. [e] The bond order between the metal fragment and the bqdi ligand and its main component, the two Ru−N_{bqdi} bonds (the Ru−N_{bqdi} bond order is in parentheses).

Table 12. NPA Charges of the bqdi Ligand, the Ru Atom, and the Remaining Ligands (q_L) in the $[Ru(L)_x(bqdi)]$ Complexes (B3LYP/LanL2DZ calculations)[a]

complex	q_{bqdi} (au)	q_{Ru} (au)	q_L (au)
(**2**) $[Ru^{II}(NH_3)_2Cl_2(bqdi)]$	−0.06 (0.05)	0.67 (0.68)	−0.61 (−0.73)
(**2**$^-$) $[Ru^{II}(NH_3)_2Cl_2(bqdi)]^-$	−0.77 (−0.76)	0.70 (0.70)	−0.93 (−0.94)
(**2**$^+$)$[Ru^{III}(NH_3)_2Cl_2(bqdi)]^+$	0.45 (0.54)	0.77 (0.83)	−0.22 (−0.37)
(**6**) $[Ru^{II}(acac)_2(bqdi)]$	−0.04	1.01	−0.97
(**4**) $[Ru^{II}(opda)_2(bqdi)]^{2+}$	0.24	0.69	1.07
(**3**) $[Ru^{II}(NH_3)_4(bqdi)]^{2+}$	0.28	0.69	1.03
(**5**) $[Ru^{II}(bpy)_2(bqdi)]^{2+}$	0.28	0.70	1.02

[a] The results of the PCM calculations (in water) are shown in parenthesis.

unoccupied orbitals (mostly π^*) of the bqdi fragment, and (iii) electronic polarization of the metal fragment and the bqdi ligand. The electronic polarization of fragments is the effect of the distortion of the electron distribution of one fragment by another and includes the interactions between all permanent charges and charge multipoles and induced multipoles.

In the evaluation of donation (i) and π-back-donation (ii), the charge decomposition analysis (CDA)[118] is usually employed. However, as has recently been demonstrated,[27] this analysis gives reasonable estimates of donation and π-back-donation between molecular fragments only if their electronic polarization is absent or sufficiently small. If it is not the case, the difference between the amounts of donation and back-donation will not be equal to the net charge transfer between fragments, as calculated from the sum of atomic charges. For example, for **2**, the bqdi → Ru^{II} donation and the bqdi ← Ru^{II} π-back-donation as derived by CDA are 0.58 and 0.22 electrons, respectively. This implies that the donation is greater than the back-donation and that the bqdi ligand has to carry the positive charge in the complex. However, this is not the case,; the bqdi ligand has the negative charge (MPA charge is −0.14 au (Table 11), and the NPA charge is −0.06 au (Table 12)). Thus, for $[Ru(NH_3)_2Cl_2(bqdi)]$, CDA underestimates the extent of metal-to-ligand π-back-donation relative to ligand-to-metal donation. To address this problem in a general sense, an extended CDA (ECDA) scheme has been developed by one of the authors (S.I.G.) and is employed in this work. In ECDA, by using the linear combination of fragment molecular orbitals (LCFO−MO) framework, it is possible to analyze CT and polarization contributions separately (Table 11) and to construct the MO interaction diagrams (Figure 8) that allow one to easily identify the orbital interactions relevant for chemical bonding.[27]

In **2**, the bqdi → Ru^{II} donation is produced by the interactions involving fragment orbitals of a_1 and b_2 symmetries, namely, HOMO−1 and HOMO−2 of the bqdi ligand and the LUMO and LUMO+1 of the $Ru^{II}(NH_3)_2Cl_2$ fragment (Figure 8). ECDA indicates that the populations of the LUFO and LUFO+1 of the $Ru^{II}(NH_3)_2Cl_2$ fragment in the complex are 0.42 and 0.25 electrons, respectively, while HOFO−1 and HOFO−2 of the bqdi ligand are depopulated by 0.38 and 0.20 electrons, respectively.

The bqdi ← Ru^{II} π-back-donation is almost exclusively produced by the interaction between the HOFO of the $Ru^{II}(NH_3)_2Cl_2$ fragment ($HOFO_{Ru}$) and the LUFO of the bqdi ligand ($LUFO_{bqdi}$), both of b_1 symmetry (Figure 8). The LUMO of $[Ru(NH_3)_2Cl_2(bqdi)]$ is an antibonding combination of 62% $LUFO_{bqdi}$ and 33% $HOFO_{Ru}$. The corresponding bonding orbital (HOMO−1) is formed by 61% $HOFO_{Ru}$ and 29% $LUFO_{bqdi}$. These orbital contributions indicate the strong π-back-bonding interaction and account for a transfer of ∼0.7 e^- (Table 11) from the $Ru^{II}(NH_3)_2Cl_2$ fragment to the bqdi ligand. Similar strong π-back-donation is present in $[Ru(acac)_2(bqdi)]$ (Table 11). These two complexes also have the most negative charge on the bqdi ligand (Table 12). The $[Ru^{II}(NH_3)_5(NO^+)]^{3+}$ species (**12**), where Ru^{II} π-back-donation to the strong π acceptor ligand, can be expected to be large and also to show a high Ru 4dπ contribution to the LUMO, and as a result of the strong π-back-donation, the NO^+ ligand carries a fairly small positive charge (0.24 au) in the complex.

Table 11 shows that the net charge donation from bqdi to the metal fragment in the other Ru complexes with less covalent Ru−bqdi bonds in the series is positive (the bqdi-to-metal donation is stronger than the metal-to-bqdi π-back-donation) and becomes slightly negative for the species **2** and **6** (the donation and the back-donation are of similar magnitude). This conclusion is also supported by natural population analysis (NPA, Table 12).

(118) Dapprich, S.; Frenking, G. *J. Phys. Chem.* **1995**, *99*, 9352.

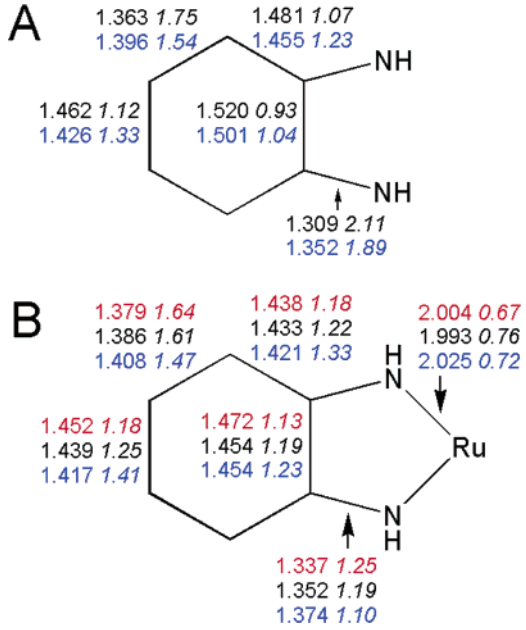

Figure 12. (top) Bond lengths (Å) and bond orders in free bqdi (black) and bqdi$^-$ (blue) ligands; (bottom) bond lengths (Å) and bond orders of the Ru-bqdi fragment in $[Ru(NH_3)_2Cl_2(bqdi)]^+$ (red), $[Ru(NH_3)_2Cl_2(bqdi)]$ (black), and $[Ru(NH_3)_2Cl_2(bqdi)]^-$ (blue). Bond orders are shown in italics.

The calculated Mayer bond orders between the RuL_x fragment and the bqdi ligand in the series clearly indicate two Ru−N covalent bonds with contributions of both bqdi → Ru^{II} donation and bqdi ← Ru^{II} π-back-donation (Table 11). In **2**, these contributions are 0.64 from the orbitals with a_1 symmetry (mostly σ donation), 0.62 from the MOs with b_2 symmetry, and 0.94 from the MOs with b_1 symmetry (mostly π-back-donation; obtained using the AOMix-L program).[24] The covalent contributions to the Ru−bqdi bonding from the orbitals with a_2 symmetry are negligible. The $[Ru(NH_3)_2Cl_2(bqdi)]$ and $[Ru(acac)_2(bqdi)]$ complexes, having the strongest bqdi ← Ru^{II} π-back-donation, show the largest $Ru-N_{bqdi}$ and RuL_x−bqdi bond orders (Table 11) and indicate the most covalent Ru−bqdi bonding in the series. The difference of 0.92 between the $C-N_H$ bond orders in the free bqdi fragment (2.11, Figure 12) and in **2** (1.19) indicates that formation of the $Ru-N_{bqdi}$ bond is accompanied by reduction of the $C-N_H$ double-bond character.

Carugo[119] analyzed the bond distances in the bqdi ligand for a range of complexes, of known X-ray structure, to derive a semi-weighted averaged value which was used to delineate a measure of the oxidation state of the ligand (i.e., to fall within the range of fully oxidized quinone (Q), intermediate semiquinone (Sq), or fully reduced diamide). This empirical scheme apparently allows one to draw conclusions about the oxidation state of the ligand in complexes where delocalization causes uncertainty (e.g., M^{II}−Q versus M^{III}−Sq). Species **2**, by this measure, is in the M^{III}−Sq regime (semi-weighted average $\Delta = 1.03$ Å) However, our DFT calculations of **2** and the corresponding reduced and oxidized complexes ($[Ru(NH_3)_2Cl_2(bqdi)]^-$ and $[Ru(NH_3)_2Cl_2(bqdi)]^+$, respectively) indicate that the best representation of the title species is Ru^{II}−Q, while for the reduced and oxidized species, the appropriate descriptions are Ru^{II}−Sq and Ru^{III}−Q, respectively. This can be seen from the NPA-derived charges (Table 12) of the bqdi ligand and the Ru atom and the bond lengths and orders of the bqdi ligand (Figure 12). $[Ru(NH_3)_2Cl_2(bqdi)]$ and its oxidized species both show the Q-like ligand structure with the alternating C−C and C═C bonds in the bqdi ring. The reduced $[Ru(NH_3)_2Cl_2(bqdi)]^-$ species shows a clear trend toward aromatic $C-C_{bqdi}$ bonds (with the bond order approaching 1.5), $C-N_{bqdi}$ single bonds, and longer less-covalent $Ru-N_{bqdi}$ bonds.

Caution should therefore be exercised in drawing conclusions about electron distribution from X-ray bond distance analyses, especially in the cases where several types of metal−ligand bonding (ionic vs covalent interactions and ligand-to-metal donation vs metal-to-ligand π-back-donation) are at play.

Solvent Effects. The calculations above refer to the gas phase. We discuss below calculations which incorporate solvent effects on species **2**. The visible region ^{1}MLCT3 transition is not solvatochromic, both energy and intensity are largely independent of solvent. We are interested to know how solvation will affect charge distribution in the Ru−bqdi complexes and the contributions to covalent bonding as derived in ECDA. The solvent will stabilize the negative charge on the chlorine ligands, and this would have the effect of making the ruthenium a little less electron rich and hence reduce the bqdi ← Ru^{II} π-back-donation. However H-bonding between the NH_3 ligands of the complex and the solvent would have the reverse effect since it would make these NH_3 ligands slightly better σ donors.

We have included solvation by optimizing the geometry of species **2** using the dielectric continuum model with solvent parameters corresponding to water ($\epsilon = 78$).[53,54] The bond distances are shown in Figure 1c and Table 2. The inclusion of the reaction field of water has little effect on any of the distances except for the Ru−Cl bonds which are elongated by about 0.03 Å from the gas-phase-optimized values.

In the PCM calculation of **2**, which does not take H-bonding effects into account, the Ru dπ contribution to the LUMO is reduced from 31.9 (gas-phase value) to 28.8%. The NPA charge of the bqdi fragment (Table 12) increases from −0.06 to 0.05 au, which indicates that bqdi ← Ru^{II} π-back-donation is now slightly less than bqdi → Ru^{II} donation, and the bond order between the RuL and bqdi fragments is now 2.13 versus 2.22 in the gas phase.

The electronic spectrum from a TD-DFT/PCM calculation is shown in Figure 4. There is no significant effect on the energy of MLCT3 but, as anticipated, the Cl → bqdi π^* transition shifts to higher energy. Thus, inclusion of solvent at the PCM level does reduce the derived π-back-donation to a small degree but the overall picture discussed in this contribution remains unchanged.

Conclusions. The noninnocent bqdi ligand is able to adjust in a dramatic fashion to an increase in electron density at the ruthenium atom, generated by replacing fairly poor electron donor (spectator) ligands, such as 2,2′-bipyridine,

(119) Carugo, O.; Djinovi, K.; Rizzi, M.; Castellani, C. B. *J. Chem. Soc., Dalton Trans.* **1991**, 1551.

with good donors, such as chloride or acetylacetonate. Indeed the magnitude of the bqdi ← Ru^{II} π-back-donation increases and becomes greater (at least, as far as charge distribution in the complex is concerned) than the bqdi → Ru^{II} donation. Thus, the increased Ru−bqdi bond covalency (reflected in the increased $Ru-N_{bqdi}$ bond order) caused by greater bqdi ← Ru^{II} π-back-donation causes the $Ru-N_{bqdi}$ bonds to shorten significantly.

The greater Ru 4dπ contribution to the LUMO leads to a decrease in the CT character of the MLCT3 transition reflected in a lack of solvatochromism in this transition. The substantial increase in π-back-donation was also revealed by the apparent E_L(L) value of the bqdi ligand which increases dramatically as the donicity of the spectator ligands increases rather than remaining constant as is the normal situation for "innocent" ligands. Increasing π-back-donation to the bqdi ligand also caused a significant negative shift in the potential required to reduce the complexed ligand, changing in a linear fashion with the $\sum E_L$(L) value of the spectator ligands.

RR spectroscopy proved to be of great value in this study revealing considerable enhancement of the $Ru-NH_{bqdi}$ stretching vibration and observation of a significant progression in this vibration (to n=5). This vibration is coupled to the intrametallacycle C═NH stretching vibration. In combination with a DFT analysis of the displacements of the enhanced Raman vibrations, we argued that the MLCT3 excitation occurs only as far as the metallacycle ring with little perturbation of the bqdi ring. This was then linked to a marked increase in the exchange integral associated with this electron excitation. This increase in the exchange integral then contributed in a major fashion to the increased value of C in eq 6b and this, it was argued, was the result of a marked increase in the magnitude of the parameter Q (eq 6a and 7). Further, the increase in the exchange integral for MLCT3 causes a greater separation between the energy of this transition and the energies of ^{1}MLCT1,2 making the latter very weak transitions easier to observe.

Thus, it was possible to understand the changes in the electrochemistry, optical spectroscopy and vibrational spectra with changing spectator ligand donor ability within a common theoretical (DFT) model which further provided a detailed analysis of the variation in the molecular orbital descriptions. A detailed picture emerged of the coupling between the bqdi ligand and the remaining ruthenium fragment illustrating the coupling between the MOs of each fragment as a function of orbital symmetry.

ECDA proves itself to be a powerful adjunct to understanding the electron distribution in these complexes since it permits one to quantify in some considerable detail the changes in charge distribution which occur at the bqdi ligand and ruthenium fragment, as the spectator ligands are varied. As more species are analyzed by ECDA, a more detailed understanding of metal−ligand interactions may emerge.

Strongly coupled complexes such as species **2** compose a new class of coordination compound wherein the Ru−L covalency is becoming comparable to the C−C bond covalency.

Acknowledgment. A.B.P.L. and C.R. thank the Natural Science and Engineering Research Council (NSERC, Ottawa) for financial support. S.I.G. also thanks NSERC for a Postdoctoral Fellowship. We also thank Dr. Nicholas C. Payne (University of Western Ontario) for crystallographic assistance and Dr. Rowshan Begum for experimental assistance.

Supporting Information Available: Crystal packing data for compounds **1** and **2**, cyclic voltammogram of **1**, composition of molecular orbital for **2**, more detailed resonance Raman data for **2** with DFT predicted vibrational energies, the TD-DFT and INDO/S calculated electronic spectra, and the optimized atomic coordinates and CIF files of **1** and **2**. CHIME-readable xyz files of the DFT optimized structures of species **1** and **2** are also included. This material is available free of charge via the Internet at http://pubs.acs.org.

IC060220Z